

Machine learning a time-local fluctuation theorem for nonequilibrium steady states

Stephen Sanderson¹, Charlotte F. Petersen^{1,2}, and Debra J. Searles^{1,3,*}

¹Australian Institute for Bioengineering and Nanotechnology, The University of Queensland, Brisbane, QLD, 4072, Australia

²School of Chemistry, University of Melbourne, Melbourne, Victoria, 3010, Australia

³School of Chemistry and Molecular Biosciences, The University of Queensland, Brisbane, QLD, 4072, Australia
*d.bernhardt@uq.edu.au

ABSTRACT

Fluctuation theorems (FTs) quantify the thermodynamic reversibility of a system, and for deterministic systems they are defined in terms of the dissipation function. However, in a nonequilibrium steady state of deterministic dynamics, the phase space distribution is unknown, making the dissipation function difficult to evaluate without extra information. As such, steady state FTs for deterministic systems to date have required either that the trajectory segment of interest is relatively long, or that information is available about the entire trajectory surrounding that segment. In this work, it is shown that a simple machine learning model trained to predict whether a given steady state trajectory segment is being played forward or backward in time calculates a function which satisfies an FT and relies solely on information within the segment of interest. The FT is satisfied even for very short trajectory segments where the approximate relation derived from theory breaks down, for systems far from equilibrium, and for various nonequilibrium dynamics. It is further demonstrated that any function which is a well-calibrated predictor of time's arrow must satisfy a fluctuation theorem, and that a local FT can be derived which depends only on local dissipation and its correlations with the surrounding non-local dissipation.

1 Introduction

Nonequilibrium processes are ubiquitous in nature and everyday life, yet our understanding of them from a thermodynamics perspective is limited. One of the few thermodynamic relations that is valid arbitrarily far from equilibrium is the fluctuation theorem (FT) that quantifies the probability of observing, over some period of time, events that violate the 2nd law of thermodynamics [1]. The FT of Evans and Searles [2, 3], which is applicable to deterministic dynamics, has been used to derive a number of useful relations. This includes the Green-Kubo relations for transport properties, and the dissipation theorem, which gives the average value of a phase function arbitrarily near or far from equilibrium and can achieve greater accuracy over shorter time periods or under smaller driving forces in comparison to direct averaging techniques [1, 4–7]. However, the FT for deterministic dynamics can only be exactly evaluated under the condition that the distribution function of the initial ensemble from which the nonequilibrium trajectories begin is a known (typically equilibrium) one. Often we are interested in nonequilibrium steady state systems which are either approximately characterised by a continuously changing phase distribution function after the phase variables have reached their steady state values to within a desired tolerance, or by a steady state measure that might not be a function. For these systems, if only time-local information is known, the FT can only be evaluated as an approximate relation that is asymptotically valid as the duration of the measurement increases [1].

The broad umbrella of nonequilibrium steady state systems encompasses many important processes

across various fields, including fluid flow, heat transfer, semiconductor operation, ion transport, biological phenomena, and climate modelling [8–14]. For many systems to function, it is necessary that they are maintained in a state other than the equilibrium one, requiring application of a constant driving force or flux and leading to a nonequilibrium steady state. Hence, the discovery of improved theory for treating nonequilibrium steady states could have a wide impact.

With the growing capabilities of machine learning and artificial intelligence, it has become apparent that such models can prove an effective tool for gaining new and interesting scientific understanding [15, 16]. Notably, it was recently demonstrated by Sief *et al.* that a machine learning model is capable of rediscovering the Crooks FT for transient stochastic dynamics [17]. In this work, we apply simple machine learning techniques to non-equilibrium steady states. Our model discovers a steady state fluctuation theorem for deterministic dynamics that remains valid even for very short measurements and is more accurate than previously known relationships.

2 Background

2.1 Steady-state fluctuation theorems

The fluctuation theorem quantifies the reversibility of a system as [3]

$$\ln \frac{p(\Omega_{0,t}(\Gamma;0) = At)}{p(\Omega_{0,t}(\Gamma;0) = -At)} \equiv \ln \frac{p(\bar{\Omega}_{0,t}(\Gamma;0) = A)}{p(\bar{\Omega}_{0,t}(\Gamma;0) = -A)} = At, \quad (1)$$

where $\Omega_{0,t}(\Gamma;0)$ is the dissipation function of the trajectory of the phase space vector, Γ , integrated between time 0 and time t , defined with respect to the phase space distribution at time 0, and $p(\Omega_{0,t}(\Gamma;0) = At)$ is the probability that a trajectory has the particular dissipation value At . The symbol $\bar{\Omega}$ denotes the time averaged value over the indicated segment.

In general, the time integral of the dissipation function of a trajectory segment from time t_1 to time t_2 is given by

$$\Omega_{t_1,t_2}(\Gamma;t_d) \equiv \ln \frac{f(\Gamma_{t_1};t_d)}{f(M^T\Gamma_{t_2};t_d)} - \int_{t_1}^{t_2} \Lambda(\Gamma_s)ds, \quad (2)$$

where $f(\Gamma_t;t_d)$ is the phase space probability density of the system at time t_d , evaluated at the point Γ_t . Γ_t is a point in phase space at time t , which is independent of t_d . M^T is a time-reversal mapping,[†] and

$$\Lambda(\Gamma) \equiv \frac{\partial}{\partial \Gamma} \cdot \dot{\Gamma} \quad (3)$$

is the phase space expansion factor [3]. For the dissipation function to satisfy the fluctuation theorem in the form of Equation 1, it must be integrated from the same time as the distribution relative to which it is defined; that is, $t_d = t_1$. Furthermore, in order to evaluate the dissipation function, the phase space distribution function at t_d must be well defined, which is not the case for trajectory segments beginning from a nonequilibrium steady state.

There are two common approaches towards obtaining the steady state FT (SSFT) from consideration of transients (trajectories beginning from $t = 0$). Firstly, consider the case where the distribution function

[†]More generally, this is the mapping required so that when the system is subject to the same driving force, the dynamics will generate a trajectory with an integrated dissipation of the same magnitude but opposite sign. The mapping is often $\{\mathbf{q}, \mathbf{p}\} \rightarrow \{\mathbf{q}, -\mathbf{p}\}$, but exceptions include shear flow [18], considered in Section 4.3, and when a magnetic field is considered [19].

is known at $t = 0$ (e.g. it is an equilibrium distribution) and the system is evolving towards a steady state. Noting that [1]

$$\Omega_{t,t+\tau}(\Gamma;t) = \Omega_{0,2t+\tau}(\Gamma;0), \quad (4)$$

and hence,

$$\tau\bar{\Omega}_{t,t+\tau}(\Gamma;t) = (2t + \tau)\bar{\Omega}_{0,2t+\tau}(\Gamma;0), \quad (5)$$

one can use knowledge of the surrounding periods of the trajectory to define an exact SSFT as [1]

$$\begin{aligned} \ln \frac{p(\bar{\Omega}_{t,t+\tau}(\Gamma;t) = A)}{p(\bar{\Omega}_{t,t+\tau}(\Gamma;t) = -A)} &= \ln \frac{p(\bar{\Omega}_{0,2t+\tau}(\Gamma;0) = \frac{A\tau}{2t+\tau})}{p(\bar{\Omega}_{0,2t+\tau}(\Gamma;0) = -\frac{A\tau}{2t+\tau})} \\ &= A\tau. \end{aligned} \quad (6)$$

Although this is an exact expression, it is generally not of practical use. This is because the dissipation function on the left hand side is defined with respect to the time-evolved distribution at time t , and the dissipation function on the right hand side requires knowledge of the trajectory outside the period of interest. If only time-local information is available and/or $t \rightarrow \infty$, this is problematic.

Alternatively, noting that

$$\Omega_{t,t+\tau}(\Gamma;0) = \Omega_{0,\tau}(\Gamma;0) + \Omega_{\tau,\tau+t}(\Gamma;0) - \Omega_{0,t}(\Gamma;0), \quad (7)$$

if we can assume that correlations decay sufficiently quickly (the system is T-mixing [1]) and select t to be much greater than τ_M , the Maxwell time of the system which characterises time correlations, then one can make the approximation that [1]

$$\bar{\Omega}_{t,t+\tau}(\Gamma;0) = \bar{\Omega}_{0,\tau}(\Gamma;0) + \mathcal{O}\left(\frac{\tau_M}{\tau}\right). \quad (8)$$

Hence, the approximate SSFT can be derived as [1]

$$\lim_{\tau \rightarrow \infty} \frac{1}{\tau} \ln \frac{p(\Omega_{t,t+\tau}(\Gamma;0) = A\tau)}{p(\Omega_{t,t+\tau}(\Gamma;0) = -A\tau)} = A, \quad (9)$$

provided the standard deviation of the distribution of values, A , shrinks less quickly than $1/\tau$. Then, the steady state dissipation function defined with respect to the initial, known distribution satisfies the fluctuation theorem in the limit that the trajectory segment of interest is much longer than the correlation time. However, for small τ this limit does not apply.

A similar problem is encountered when deriving the SSFT from the functional FT [1, 20, 21],

$$\frac{p(F(\Gamma_{0 \rightarrow 2t+\tau}) = A)}{p(F(\Gamma_{0 \rightarrow 2t+\tau}) = -A)} = \left\langle e^{-\Omega_{0,2t+\tau}(\Gamma;0)} \right\rangle_{F(\Gamma_{0 \rightarrow 2t+\tau}) = -A}, \quad (10)$$

where $\Gamma_{0 \rightarrow 2t+\tau}$ denotes the trajectory segment from time 0 to time $2t + \tau$, F is a path function of that segment that is odd with respect to time-reversal, and $\langle \dots \rangle_{\text{cond.}}$ denotes an ensemble average over trajectory segments that satisfy the given condition. Substituting $F(\Gamma_{0 \rightarrow 2t+\tau}) = \Omega_{t,t+\tau}(\Gamma;0)$ gives [21]

$$\frac{p(\Omega_{t,t+\tau}(\Gamma;0) = A\tau)}{p(\Omega_{t,t+\tau}(\Gamma;0) = -A\tau)} = e^{A\tau} \left\langle e^{-\Omega_{0,t}(\Gamma;0)} e^{-\Omega_{t+\tau,2t+\tau}(\Gamma;0)} \right\rangle_{\Omega_{t,t+\tau}(\Gamma;0) = -A\tau}. \quad (11)$$

For a T-mixing system with τ much greater than the Maxwell time, correlations between $\Omega_{0,t}(\Gamma;0)$, $\Omega_{t,t+\tau}(\Gamma;0)$ and $\Omega_{t+\tau,2t+\tau}(\Gamma;0)$ can be assumed to be independent of τ , in which case

$$\begin{aligned} \left\langle e^{-\Omega_{0,t}(\Gamma;0)} e^{-\Omega_{t+\tau,2t+\tau}(\Gamma;0)} \right\rangle_{\Omega_{t,t+\tau}(\Gamma;0)=-A\tau} &= \left\langle e^{-\Omega_{0,t}(\Gamma;0)} \right\rangle_{\Omega_{t,t+\tau}(\Gamma;0)=-A\tau} \times \\ &\quad \left\langle e^{-\Omega_{t+\tau,2t+\tau}(\Gamma;0)} \right\rangle_{\Omega_{t,t+\tau}(\Gamma;0)=-A\tau} \\ &= C(t), \end{aligned} \quad (12)$$

again resulting in Equation 9.

The problems encountered here are not unique to steady states, but are more generally reflective of difficulties in treating a dissipation function which is missing information. The initial distribution is unknown for trajectories beginning from a steady state, as is their time evolution from the known ($t = 0$) distribution in the case of time-local measurements. Similar difficulties are found when deriving the space-local FT for the dissipation function calculated over a local volume of a larger system, in which case the missing information is the dissipation function of the remaining volume of the system. However, although there has been some progress towards space-local fluctuation theorems through both theoretical and experimental investigations [22–27], there is currently no evaluable time-local SSFT that remains accurate for arbitrarily short trajectories.

It has been shown that if a local dissipation function is defined as $\Omega_{0,t}^L(\Gamma;0) = \Omega_{0,t}(\Gamma;0) - \Omega_{0,t}^{L'}(\Gamma;0)$, where $\Omega_{0,t}^{L'}(\Gamma;0)$ is the remaining, non-local component of the global dissipation function, then for some systems an approximate space-local FT can be obtained using a linear scaling factor α [22, 23]. This scaling factor accounts for first-order correlations between the local and non-local components such that

$$\Omega_{0,t}^{L'}(\Gamma;0) = \alpha \Omega_{0,t}^L(\Gamma;0) + \xi, \quad (13)$$

where ξ represents the uncorrelated components of $\Omega_{0,t}^{L'}(\Gamma;0)$. This gives the space-local FT [22, 23],

$$\ln \frac{p(\Omega_{0,t}^L(\Gamma;0) = At)}{p(\Omega_{0,t}^L(\Gamma;0) = -At)} = (1 + \alpha)At. \quad (14)$$

If spatial correlations are then assumed to be exponentially decaying in nature, a value of α can be calculated as [22, 23]

$$\alpha \approx \frac{l_0 \left(1 - e^{-l/l_0}\right)}{l - l_0 \left(1 - e^{-l/l_0}\right)}, \quad (15)$$

where l_0 is the correlation length, and l is the size of the local area of interest for which $\Omega_{0,t}^L(\Gamma;0)$ is defined. Although this formalism may, in principle, extend to time-locality, time correlations in $\Omega(\Gamma;0)$ may not be well represented by an exponential decay, making α difficult to calculate. Hence, an alternative approach is required.

2.2 Machine learning fluctuation theorems

One interesting property of the fluctuation theorem is that in theory it can be used to predict whether a movie of a nonequilibrium physical process is being played forward or backward. Indeed, it was recently shown by Seif *et al.* [17] that a neural network recovers a form of the Crooks FT [28] when given an equal

mix of forward and reverse, stochastic, transient trajectories as input and trained to predict the direction of time's arrow. In the present work, similar machine learning methods are employed to investigate the possibility of an accurate time-local SSFT for deterministic dynamics.

Following Crooks and Jarzynski [28, 29], for a trajectory of length τ sampled from an equal mix of forward-process and time-reversed reverse-process trajectories, the probability that it was generated by the forward process is given by

$$p_+(\Gamma_{0 \rightarrow \tau}) = \frac{1}{1 + e^{-\beta(W_{0,\tau} + \Delta F)}}, \quad (16)$$

where $W_{0,\tau}$ is the work along the trajectory from time 0 to time τ , $\beta^{-1} = k_B T$ is the inverse temperature, and ΔF is the free energy difference between the initial and final configuration of the process. See Section 1 of the supporting information for the derivation of this expression from the Crooks FT.

It is worth clarifying here that the forward and reverse processes considered when discussed with regard to Equation 1 are not necessarily synonymous with those considered when discussing the FT of Equation 16 [1]. Consider trajectories that are sampled from an initial equilibrium distribution characterised by λ_A , with $\lambda(t)$ being a parameter describing a time-dependent process driving a change in the system, with $\lambda(\tau) = \lambda_B$. A set of trajectories, $\Gamma_{0 \rightarrow \tau}$, progress from the initial equilibrium ensemble to some final (nonequilibrium) ensemble of states at τ . There will be a corresponding set of conjugate trajectories, $\Gamma_{0 \rightarrow \tau}^*$, that are related by time-reversal symmetry. If the protocol for variation of $\lambda(t)$ is not time-symmetric over the period τ , then the conjugate trajectories will be generated with the evolution of $\lambda(t)$ reversed (varying from λ_B to λ_A). The FT given by Evans and Searles, which is stated in Equation 1, quantifies the probability ratio of observing, from the *same* initial phase space distribution, a trajectory, $\Gamma_{0 \rightarrow \tau}$, and its corresponding conjugate trajectory, $\Gamma_{0 \rightarrow \tau}^*$.[‡] In contrast, the Crooks FT compares the probabilities of trajectories $\Gamma_{0 \rightarrow \tau}$ sampled from an initial equilibrium distribution characterised by λ_A and driven by $\lambda(t)$ changing to λ_B , with the probabilities of conjugate trajectories $\Gamma_{0 \rightarrow \tau}^*$ sampled from the equilibrium distribution characterised by λ_B and $\lambda(t)$ changing to λ_A with the reverse protocol.

As we are interested in deterministic systems that are subject to a constant driving force, not the transition between two equilibrium states, in this work we deal exclusively with systems for which there is no free energy difference and the time-local version of the Evans-Searles FT is an approximate relation (Equation 9). The systems we consider here are generated by time-reversible and deterministic dynamics, which differs from the equations of motion of reference [17] that are not time-reversible. Therefore it might be supposed that it is impossible to determine if the trajectory is more likely to have been sampled from a forward or reverse simulation. However, it has been observed that for steady states there is a time asymmetry in the fluctuations [30, 31], and a steady state FT is followed [2, 21, 32].

To expand on this, we note that for this type of dynamics (deterministic and reversible), any trajectory that is a solution to the equations of motion will be possible in either the forward or reverse process. So the question is not whether the trajectory was played forwards or backwards (as both are possible), but the likelihood that it was generated naturally, or after being played in reverse. See Figure S1 in the supporting information for an illustration. This is different to irreversible dynamics where a trajectory that occurs in the forward direction could be impossible in the set of trajectories played in reverse, and vice versa.

Therefore, considering Equations 5 and 9 and Section 1 of the supporting information, the probability that a trajectory is a forward one, when drawn randomly from an even mix of forward and time-reversed

[‡]Note, if the protocol for variation of λ is not time-symmetric, then the set of trajectories considered in evaluation of the probabilities in Equation 1 will include those generated with both the forward and reverse evolution of λ (i.e. from λ_A to λ_B and from λ_B to λ_A).

trajectories, is given by

$$\begin{aligned}
p_+(\Gamma_{t \rightarrow t+\tau}) &= \frac{1}{1 + e^{-\Omega_{t,t+\tau}(\Gamma;t)}} \\
&= \frac{1}{1 + e^{-\Omega_{0,2t+\tau}(\Gamma;0)}} \\
&\approx \frac{1}{1 + e^{-\Omega_{t,t+\tau}(\Gamma;0)}},
\end{aligned} \tag{17}$$

where the final result requires $\tau \gg \tau_M$, except when $t = 0$ when it becomes an equality.

3 Machine learning model

3.1 Structure

As our aim is to determine whether a machine learning model can find a new, more accurate form of the time-local SSFT for deterministic systems, we begin by constructing a model which predicts whether a given deterministic trajectory segment is being played forwards or backwards in time [17]. This binary classification model should output a value between 0 and 1, with values closer to 1 being forward predictions, while those closer to 0 are reverse predictions. Such bounding was achieved, as is common practice for binary classifiers, by applying the nonlinear sigmoid function,

$$\sigma(x) = \frac{1}{1 + e^{-x}}, \tag{18}$$

to the scalar output of the final neural network layer. Note that this is an arbitrary choice in that any sufficiently complex combination of nonlinear functions could theoretically produce an equivalent result, although a more complex neural network would likely be required in such cases to obtain equivalent accuracy.

Whereas initial models used raw trajectories (time-dependent particle positions and momenta) as input, a more complex model was required for more complicated dynamics, as was observed previously in reference [17]. It was found that by instead using samples of the instantaneous dissipation function, $\Omega(\Gamma;0)$, as input, which is defined by

$$\Omega_{t,t+\tau}(\Gamma;0) = \int_t^{t+\tau} \Omega(\Gamma_s;0) ds, \tag{19}$$

good results could be obtained even with a simple single-layer logistic regression model for all dynamics tested.

With this single-layer structure, the probability assigned by the model that a trajectory is a forward one can be written as

$$p_+^{NN}(\Gamma) = \frac{1}{1 + e^{-B_{t,t+\tau}(\Gamma)}}, \tag{20}$$

where, for input generated by molecular dynamics simulations with an integration timestep of δt ,

$$B_{t,t+\tau}(\Gamma) = \sum_{i=1}^M w_i \Omega(\Gamma_{t+i\delta t};0), \tag{21}$$

where $M = \tau/\delta t$. Note that although initial tests included a constant bias in this equation as an extra free parameter, it was found that the bias was approximately 0 in all cases, and averaged to 0 when models

were re-trained multiple times. This was as expected for a process without a free energy change when the sigmoid function is used for nonlinearity with this simple model, and hence the bias was not included in the model for any results presented here, leaving only the weights as free parameters.

To reduce the number of free parameters to N (and thereby reduce the amount of data required for good convergence), each consecutive set of $M' = M/N$ input values was summed before applying the weights, giving

$$B_{t,t+\tau}^{(N)}(\Gamma) = \sum_{i=1}^N w_i \sum_{j=1}^{M'} \Omega(\Gamma_{t+[(i-1)M'+j]\delta t}; 0), \quad (22)$$

and the associated probability

$$p_+^{NN}(\Gamma) = \frac{1}{1 + e^{-B_{t,t+\tau}^{(N)}(\Gamma)}}. \quad (23)$$

See Figure 1a for a graphical representation of the full model structure, and Figure S2 in the supporting information for confirmation that such a model is capable of reproducing the results of Seif *et al.* [17] for the transient optical tweezers experiment in the case of deterministic dynamics.

Noting that

$$\int_t^{t+M'\delta t} \Omega(\Gamma_s; 0) ds = \delta t \sum_{j=1}^{M'} \Omega(\Gamma_{t+j\delta t}; 0) + \mathcal{O}(\delta t^2), \quad (24)$$

it is clear from Equation 19 that for small δt , Equation 22 is equivalent to

$$B_{t,t+\tau}^{(N)}(\Gamma) \approx \sum_{i=1}^N \frac{w_i}{\delta t} \Omega_{t_{i-1}, t_i}(\Gamma; 0), \quad (25)$$

where $t_i = t + iM'\delta t$. Hence, the input to the model is, to a first order approximation, equivalent to consecutive, equal-length segments of the time-local dissipation function.

3.2 Training

Each data set was split into a training set (typically of 12,000 trajectories), a validation set (typically of 4,000 trajectories), and a test set (typically 84,000 trajectories). In each data set, exactly half of the trajectories were randomly chosen to be time-reversed ones. As the dynamics are deterministic, time reversal could be achieved simply by reversing the order of samples of $\Omega(\Gamma; 0)$ and inverting the sign; that is, for a particular phase point, Γ_{t+s} , at time s after the beginning of the trajectory segment $\Gamma_{t \rightarrow t+\tau}$, $\Omega(\Gamma_{t+s}; 0) = -\Omega(\Gamma_{t+\tau-s}^*; 0)$.

The machine learning model was trained using the Adam optimiser [33] to minimise the binary cross-entropy loss function [17, 34]. Note that while initial results were obtained using the L_2 regularization technique to prevent over-reliance on a single weight [34] this was ultimately disabled to ensure that it did not affect the distribution of the weights. The lack of weight over-reliance prevention did not noticeably affect the accuracy or rate of convergence for the systems tested here.

4 Test systems

Input data was generated using deterministic molecular dynamics simulations of various nonequilibrium processes as outlined below. In all cases, the equations of motion were integrated using the 4th order

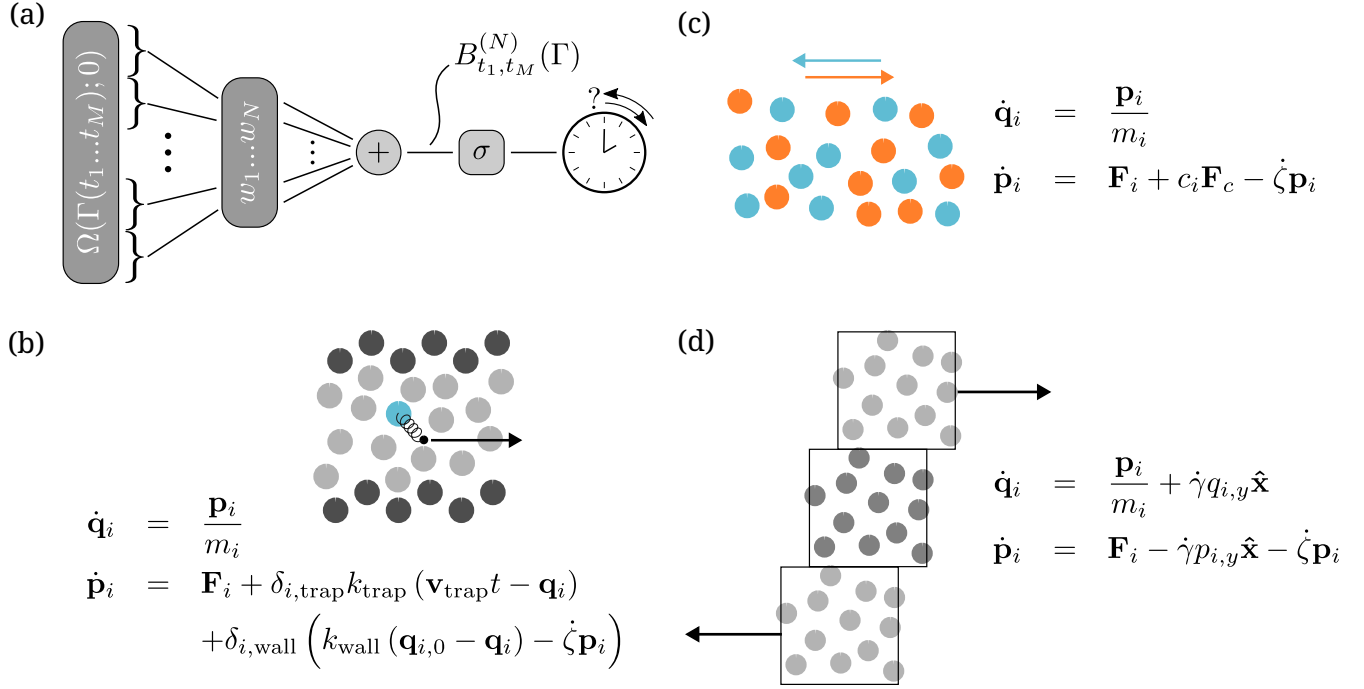


Figure 1. Graphical representation of (a) the logistic regression model, (b) the optical tweezers system in which the wall (darker) particles are harmonically restrained to a lattice, (c) the color field system, and (d) the planar shear system illustrating Lees-Edwards boundary conditions applied to the periodic images above and below the unit cell. The instantaneous dissipation function (with respect to the known initial distribution) was used as input in (a), and the sigmoid function was used for nonlinearity to allow simple comparison with the fluctuation theorem. \mathbf{q}_i and \mathbf{p}_i represent the position and momentum, respectively, of particle i , and δ is the Kronecker delta function. ζ is the thermostat coefficient governed by $\zeta = (2K_{\text{tp}}/(dN_{\text{tp}}k_{\text{B}}T) - 1)/\tau_{\text{damp}}^2$ where τ_{damp} is the time constant of the thermostat, d is the dimensionality of the system, N_{tp} is the number of thermostatted particles, equal to the number of wall particles in (a) or the total number of particles in (b) and (c), and K_{tp} is the kinetic energy of those particles. In (b), $\mathbf{q}_{i,0}$ denotes the initial lattice position of wall particle i . In (c), $q_{i,y}$ and $p_{i,y}$ denote the y component of the position and momentum of particle i , and $\hat{\mathbf{x}}$ represents the x unit vector. Note that the optical tweezers system was simulated in 2D, while the color field and shear flow systems were simulated in 3D.

Runge-Kutta method, and quantities are given in Lennard-Jones normalised units. Unless otherwise stated, the integration timestep was $\delta t = 0.001$, and temperature was controlled using a Nosé-Hoover thermostat with $k_{\text{B}}T = 1.0$ and a time constant of $100\delta t$ [35]. Initial particle velocities were sampled from a Boltzmann distribution at the same temperature as the thermostat, with any global momentum bias subtracted before beginning the simulation.

4.1 Optical tweezers

Firstly, the 2D optical tweezers experiment was used, as described in detail by Wang *et al.* [36] and represented graphically in Figure 1b. Only the wall particles were influenced by the thermostat, while the motion of the fluid particles was according to Newton's laws. A total of 44 wall particles were used, and they were harmonically restrained to their initial locations in a hexagonal lattice of number density 1.0 with a spring constant $k_{\text{wall}} = 150$. Fluid particles were initialised as part of the same lattice, and were then randomly deleted to achieve the desired fluid number density (ρ). The periodic boundaries parallel and

perpendicular to the walls were approximately of length 11.2 and 11.8 respectively. Particle interactions were of the Weeks-Chandler-Anderson (WCA) type [37]. One fluid particle close to the middle of the channel was chosen to be influenced by a harmonic trap (of spring constant k_{trap}), which was located equidistant from the walls. The system was then equilibrated for 1 million timesteps before beginning the nonequilibrium process, at which point the harmonic trap began moving parallel to the walls with constant velocity \mathbf{v}_{trap} . The instantaneous dissipation function in this experiment is given by

$$\Omega(\Gamma; 0) = -\beta \mathbf{F}_{\text{trap}} \cdot \mathbf{v}_{\text{trap}}, \quad (26)$$

where \mathbf{F}_{trap} is the force on the trapped particle due to the harmonic restraint [36].

4.2 Color field

Second was a color field experiment, shown pictorially in Figure 1c, in which half of the particles were assigned a color ‘charge’, c_i , of -1 while the other half are assigned +1. These color charges interact only with an external field, \mathbf{F}_c , driving differently colored particles in opposite directions to each other with a force of $c_i \mathbf{F}_c$ [4, 38]. Particle interactions were again of the WCA type, with a total of $N_p = 96$ particles in a 3D, periodic, cubic simulation box scaled to give a number density of $\rho = 0.7$. All particles were influenced by the Nosé-Hoover thermostat, and were equilibrated for 1 million timesteps before applying the external field. The instantaneous dissipation function of this system is given by the ‘color current’,

$$\Omega(\Gamma; 0) = \beta \sum_{i=1}^{N_p} c_i \mathbf{v}_i \cdot \mathbf{F}_c, \quad (27)$$

where \mathbf{v}_i is the velocity of particle i .

4.3 Shear flow

Finally, 3D planar shear flow was simulated using the SLLOD algorithm [4] with Lees-Edwards boundary conditions [39], as illustrated in Figure 1d. A shear rate of $\dot{\gamma} = \frac{dv_x}{dy} = 0.1$ was used, with particles within a cut-off radius of 2.6 interacting via the 12-6 Lennard-Jones potential ($\sigma_{LJ} = 1.0$, $\epsilon = 1.0$). 128 particles were initialised in a hexagonal close-packed (HCP) lattice at a number density of 0.6, with periodic dimensions of $5.32 \times 9.22 \times 4.35$ in the x , y , and z dimensions respectively ($4 \times 4 \times 2$ unit cells), giving a total of 128 particles. They were then allowed to equilibrate in the absence of shear (to the NVT ensemble) for 10,000 timesteps before beginning the nonequilibrium protocol. Here, the instantaneous dissipation function is given by

$$\Omega(\Gamma; 0) = -\beta \dot{\gamma} V P_{xy}(\Gamma_s), \quad (28)$$

where V is the volume of the simulation box, and P_{xy} is the xy component of the pressure tensor [40].

5 Results and discussion

We first discuss the case of applying the model to the optical tweezers experiment. It is immediately apparent from Figure 2 that the model is able to make predictions of time’s arrow that are more accurate than what can be achieved with $\Omega_{t,t+\tau}(\Gamma; 0)$. In addition, panels a and b of Figure 3 show that the value calculated by the model appears to satisfy the FT,

$$\ln \frac{p(B_{t,t+\tau}^{(N)}(\Gamma) = A\tau)}{p(B_{t,t+\tau}^{(N)}(\Gamma) = -A\tau)} = A\tau, \quad (29)$$

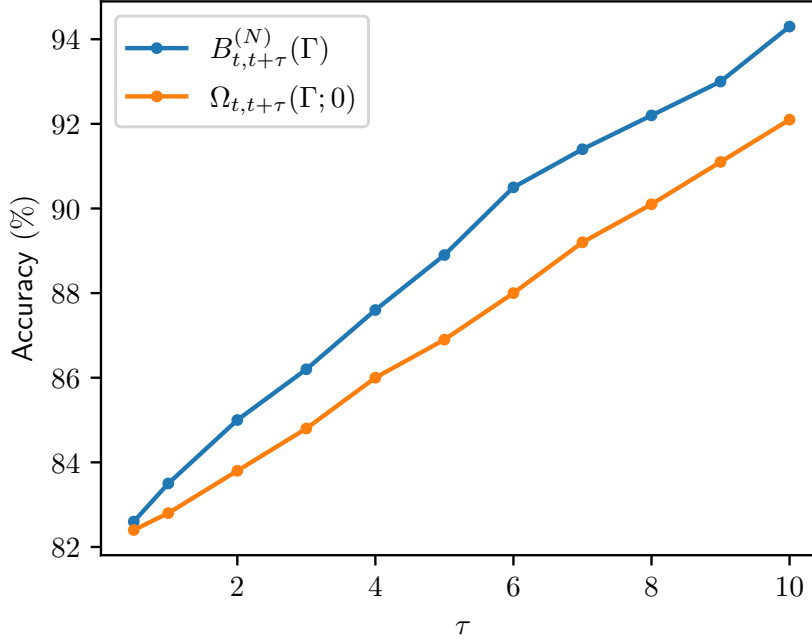


Figure 2. Predictive accuracy of the logistic regression model as a function of τ , compared against the accuracy when predictions were made from the expression $p_+(\Gamma) = \sigma(\Omega_{t,t+\tau}(\Gamma; 0))$, as per the approximate SSFT. Input trajectories of length τ were generated from the 2D optical tweezers experiment with $\rho = 0.4$, $\nu_{\text{trap}} = 0.5$, $k_{\text{trap}} = 1.0$, and $k_B T = 1.0$. They were divided into segments such that $N = \tau/50\delta t$; that is, each input value to the network was the sum of the instantaneous dissipation function over 50 consecutive simulation timesteps.

even under conditions where the approximate FT for $\Omega_{t,t+\tau}(\Gamma; 0)$ breaks down. Since the steady state FT is only expected to be true in the limit of long τ [21], this difference is most apparent for very short durations. For example, Figure 3b shows that $B_{t,t+\tau}^{(N)}(\Gamma)$ satisfies the FT even for a trajectory of length 0.003 time units; much shorter than the correlation time of $\Omega(\Gamma; 0)$, and equivalent to only three simulation timesteps ($\delta t = 0.001$). This suggests that the FT for $B_{t,t+\tau}^{(N)}(\Gamma)$ is valid for arbitrarily short durations, which is interesting as it implies that the neural network can learn the approximation that is made in obtaining the final line of Equation 17. The relation was also observed to be valid for systems closer to or further from equilibrium (Figure 3c-d), and for systems other than the optical tweezers experiment (Figure 3e-f). Note that although using fewer than 3 simulation timesteps was found to result in some error in the FT, the same dynamics and duration under a smaller integration timestep ($\delta t = 0.0005$) still produced a model that satisfied the FT. Hence, the error can be attributed to the approximate integration of the dissipation function in Equation 25.

Similar arguments to those presented in reference [41] indicate that for systems where τ is less than or similar to τ_M , correlations with periods either side of the segment $\Gamma_{t \rightarrow t+\tau}$ might be expected to result in a FT of the form

$$\ln \frac{p(\Omega_{t,t+\tau}(\Gamma; 0) = A\tau)}{p(\Omega_{t,t+\tau}(\Gamma; 0) = -A\tau)} \approx A(\tau + c\tau_M) = A\tau(1 + c\frac{\tau_M}{\tau}), \quad (30)$$

where c is a constant, at least for values of A that are close to the mean. This is equivalent to the introduction

of a scaling factor, $(1 + \alpha)$, and corresponds to the approach assumed and demonstrated in the space-local FT (Equation 14) [22, 23]. Considering the plots in Figure 3, this would result in straight lines of slope $1 + c\tau_M/\tau$ which would deviate greatly from the time-asymptotic result of 1 when τ is short, as is evident in the figure. However, using the same argument, the predictive accuracy of the approximate SSFT would only change slightly. This can be seen by considering how $p_+(\Gamma_{t \rightarrow t+\tau})$ would change with c under this approximation. Thus the predictive accuracy of $\Omega_{t,t+\tau}(\Gamma; 0)$ is similar to that of $B_{t,t+\tau}(\Gamma)$ even when the FT are very different, as is evident in the results for small τ presented in Figures 2, 3b and 3d.

For systems very far from equilibrium where $p(\Omega_{t,t+\tau}(\Gamma; 0) < 0)$ is very small, a model that satisfies the FT is still theoretically possible (see the discussion below), but is not practically feasible to train, or even to plot the FT, due to the enormous amount of data that would be required in order to include the rare but necessary 2nd law-violating trajectories. Similarly, for systems very close to equilibrium, (Figure 3c for example), training of the model becomes more difficult due to the large amount of overlap in the distribution of the time-local dissipation function between the forward and reverse sets of trajectories. In the latter case, a combination of larger data sets and a slower learning rate was required to obtain good results.

5.1 Limited information

To understand which features of the input are important, we now explore the effects of limited information on the predictive accuracy, and on the accuracy with which the FT is satisfied. First, models were trained under the condition that the order of the inputs were randomly permuted for each trajectory, thereby removing information about causality. We denote the value calculated by these models as $B_{t,t+\tau}^{(N^*)}(\Gamma)$, and for models where the number of weights was less than the number of timesteps ($M' > 1$), consecutive timesteps were first summed before random permutation. Interestingly, this random permutation of the input had no obvious effect on the accuracy with which the FT was satisfied, as can be seen in Figure 4a. However, it did limit the predictive accuracy to within margin of error of $\Omega_{t,t+\tau}(\Gamma; 0)$, suggesting that the higher predictive accuracy of the initial model was achieved by taking advantage of the information about causality of the input data. This result also suggests that the predictive accuracy is only a measure of the amount of information available, and optimal accuracy is not required for the FT to be satisfied.

It was also observed that re-training the model multiple times on randomly permuted data resulted in different weights each time, indicating that only the distribution of the weights was important for the FT to be satisfied. To confirm this, the network was re-trained 100 times on the same set of data (with different random permutations each training epoch) to determine the cumulative distribution function (CDF) of the weights. A new set of weights was then sampled from that CDF and applied to the same test data. Figure 4c shows that the FT was still approximately satisfied, although not quite as accurately due to the possibility of an ‘unlucky’ set of weights that were not a good representation of the distribution. However, Figure 4d shows that the effect of ‘unlucky’ sets of weights can be nullified by re-sampling the weights for each trajectory. Interestingly, although replacing the measured CDF with a Gaussian distribution having the same mean and variance and sampling a single set of weights does not accurately satisfy the FT (Figure 4e), it was still satisfied if those Gaussian weights were re-sampled per trajectory (Figure 4f).

These results show that without information about causality, only the total dissipation in the trajectory segment, $\Omega_{t,t+\tau}(\Gamma; 0)$, is important for the prediction, not the distribution of values. This can be explained as follows. Consider the value of $B_{t,t+\tau}^{(N)}(\Gamma_p)$ for any particular trajectory given by Γ_p ,

$$B_{t,t+\tau}^{(N)}(\Gamma_p) = \sum_{i=1}^N \frac{w_i}{\delta t} \Omega_{t_{i-1}, t_i}(\Gamma_p; 0). \quad (31)$$

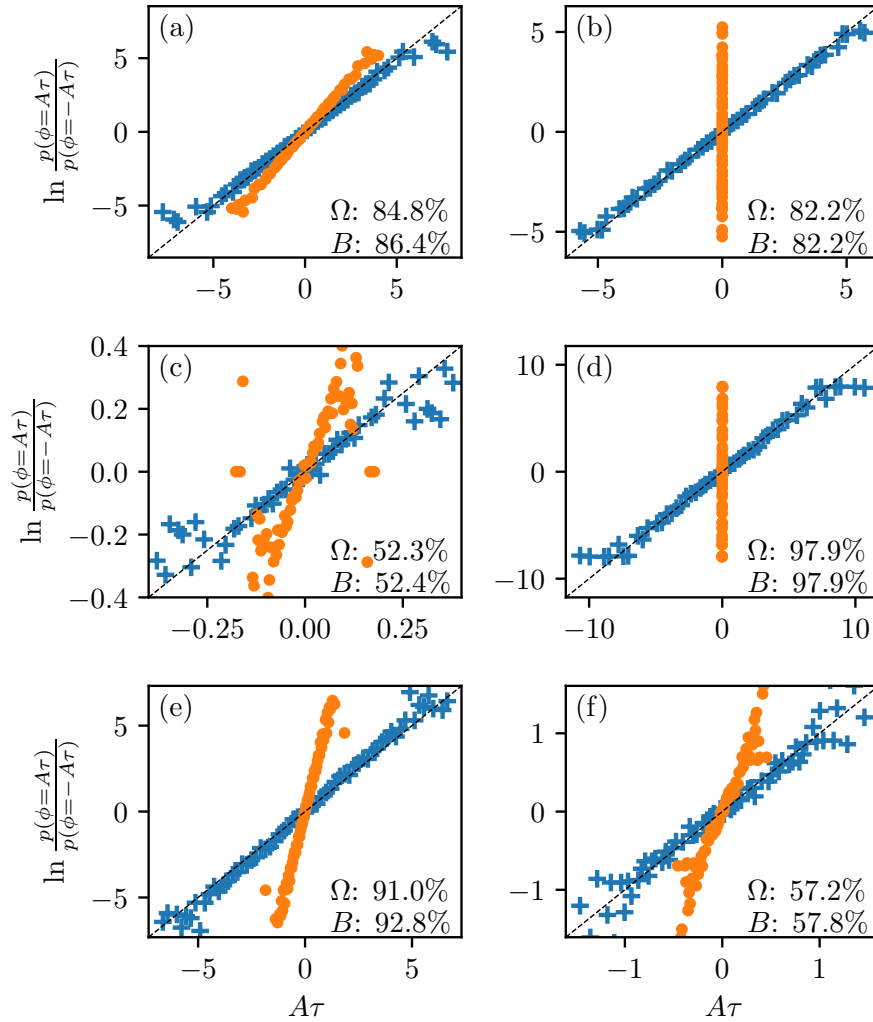


Figure 3. Test of the FT comparing $\phi = \Omega_{t,t+\tau}(\Gamma;0)$ (orange dots), and the quantity calculated by the model, $\phi = B_{t,t+\tau}^{(N)}(\Gamma)$ (blue crosses), for (a) the optical tweezers experiment with $\rho = 0.4$, $v_{\text{trap}} = 0.5$, $k_{\text{trap}} = 1.0$, $\tau = 3$ and $N = 100$, and (b) the same experiment with a duration of $\tau = 0.003$ and $N = 3$. (c) and (d) compare the FT under the same experiment close to equilibrium ($v_{\text{trap}} = 0.05$, $\tau = 0.8$, $N = 100$), and far from equilibrium ($v_{\text{trap}} = 2.0$, $\tau = 0.005$, $\delta t = 0.0005$, $N = 5$) respectively. (e) shows the same for the SLLD equations of motion with $\dot{\gamma} = 0.5$, $\tau = 0.1$, $\rho = 0.6$ and $N = 100$, and (f) shows results for the color field experiment with $N = 100$, $F_c = 0.1$ and $\tau = 0.1$ at a number density of $\rho = 0.7$. Dashed lines are a guide to the eye, showing the expected relation. The predictive accuracies of $\Omega_{t,t+\tau}(\Gamma;0)$ and $B_{t,t+\tau}(\Gamma)$ are given in the lower right corner of each plot (note the magnitude is related to the distance from equilibrium and the duration).

Since the weights, w_i , are re-sampled periodically and are uncorrelated, the average value for a given Γ_p is

$$\begin{aligned}\langle B_{t,t+\tau}^{(N)}(\Gamma_p) \rangle &= \frac{\langle w \rangle}{\delta t} \sum_{i=1}^N \Omega_{t_{i-1},t_i}(\Gamma_p; 0), \\ &\approx \frac{\langle w \rangle}{\delta t} \Omega_{t,t+\tau}(\Gamma_p; 0),\end{aligned}\quad (32)$$

where the final line is an approximate relation following from Equation 25. Hence, it is evident that sampling random weights with a mean value of $\langle w \rangle$ is equivalent to a single weight equal to $\langle w \rangle$ in the limit of a large number of samples.

Similarly, for a fixed set of weights, the average value of $B_{t,t+\tau}^{(N)}(\Gamma)$ for the set of trajectories, S , with $\Omega_{t,t+\tau}(\Gamma; 0) = A\tau$ is given by

$$\begin{aligned}\langle B_{t,t+\tau}^{(N)}(\Gamma) \rangle_S &= \left\langle \sum_{i=1}^N \frac{w_i}{\delta t} \Omega_{t_{i-1},t_i}(\Gamma; 0) \right\rangle_S, \\ &= \sum_{i=1}^N \frac{w_i}{\delta t} \langle \Omega_{t_{i-1},t_i}(\Gamma; 0) \rangle_S.\end{aligned}\quad (33)$$

If the input is randomly permuted, then at steady state

$$\begin{aligned}\langle B_{t,t+\tau}^{(N^*)}(\Gamma) \rangle_S &= \langle \Omega_{t,t+\tau/N}(\Gamma; 0) \rangle_S \sum_{i=1}^N \frac{w_i}{\delta t} \\ &= \frac{A\tau}{N} \sum_{i=1}^N \frac{w_i}{\delta t}, \\ &= \frac{\langle w \rangle}{\delta t} A\tau,\end{aligned}\quad (34)$$

and hence this too is equivalent to a single weight in the limit of a large number of samples. Note, however, that in the case of fixed time ordering, correlations between the segments of the dissipation function and the weights mean that the two cannot be separated (i.e. Equation 34 would not necessarily be correct), and therefore there is no equivalence to a single weight. In this case, though, the predictive accuracy can exceed that of $\Omega_{t,t+\tau}(\Gamma; 0)$ if the weights bias forward trajectories such that more have a positive value of $B_{t,t+\tau}^{(N)}(\Gamma)$ for a given value of $\Omega_{t,t+\tau}(\Gamma; 0)$. That is, for trajectory segments in which the direction of time's arrow is ambiguous as given by $\Omega_{t,t+\tau}(\Gamma; 0)$, a predictor that biases towards higher values for forward trajectories, or lower values for reverse trajectories, will have a higher predictive accuracy.

This phenomenon is demonstrated in Figure 5, which compares the distribution of $B_{t,t+\tau}^{(N)}(\Gamma)$ in the case of fixed time ordering with 60 segments, to that with one segment corresponding to a linear scaling factor. It can be seen that the value calculated with 60 weights, $B_{t,t+\tau}^{(60)}(\Gamma)$, has a much broader distribution than $B_{t,t+\tau}^{(1)}(\Gamma)$ for a given value range of $\Omega_{t,t+\tau}(\Gamma; 0)$, with a bias towards higher values for $\Omega_{t,t+\tau}(\Gamma; 0)$ near 0. The skewed shape of the distribution near 0 is then compensated for further from 0, where a broader range of values will still result in the same prediction (just with a different confidence), and hence the overall distribution of $B_{t,t+\tau}^{(N)}(\Gamma)$ remains one that satisfies the FT. Hence, it is evident that in the case of $B_{t,t+\tau}^{(60)}(\Gamma)$, the model is recovering extra information beyond the value of $\Omega_{t,t+\tau}(\Gamma; 0)$. This is further evidenced by the distribution of the network weights, particularly for longer trajectories, where samples of

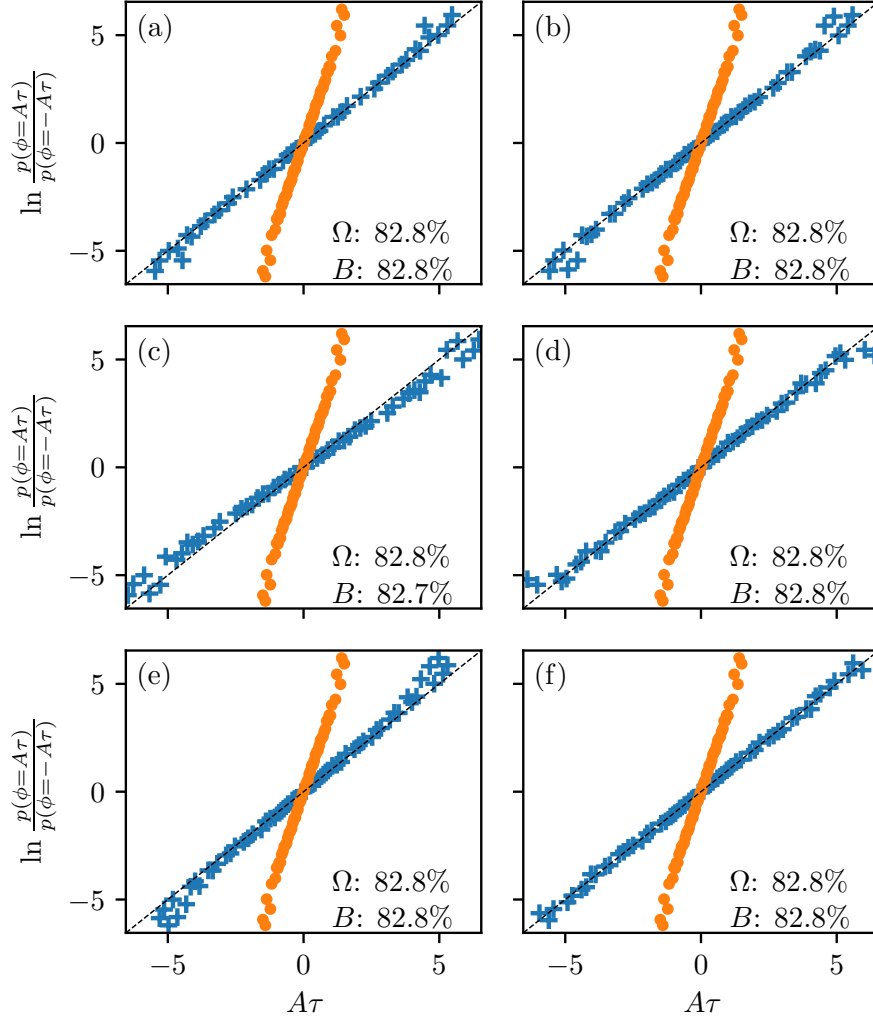


Figure 4. Test of the FT comparing $\phi = \Omega_{t,t+\tau}(\Gamma; 0)$ (orange dots), and the quantity calculated by the model, $\phi = B_{t,t+\tau}^{(N)}(\Gamma)$ (blue crosses) for the optical tweezers system with $\rho = 0.4$, $v_{\text{trap}} = 0.5$, $k_{\text{trap}} = 1.0$, and $\tau = 1$, where: (a) trajectories were randomly permuted each time they were loaded, with 20 input segments per trajectory ($N = 20$); (b) $N = 1$; (c) weights randomly sampled from the distribution of weights obtained by re-training the model considered in (a) 100 times; (d) as for (c), but with weights re-sampled per-trajectory; (e) as for (c), but sampling weights from a Gaussian distribution with the same mean and variance; and (f) as for (e), but with weights re-sampled per-trajectory. All models were trained on the same data set, and tested on the same, separate data set.

the dissipation function closer to the beginning and end of the trajectory are more heavily weighted (see Figure 6).

It is also interesting to note that the FT was satisfied even in the case that $N = 1$ (see Figure 4b). Note that $B_{t,t+\tau}^{(1)}(\Gamma)$ is just $\Omega_{t,t+\tau}(\Gamma; 0)$ multiplied by a linear scaling factor ($B_{t,t+\tau}^{(1)}(\Gamma) = \frac{w}{\delta t} \Omega_{t,t+\tau}(\Gamma; 0)$). Hence, it is apparent (at least for the systems studied in this work) that the assumption of linear correlation between the time-local and time-non-local components of the dissipation function is sufficient for a good approximation of the FT, even for very short trajectories. That is, the correlations between $\Omega_{0,t}(\Gamma; 0)$,

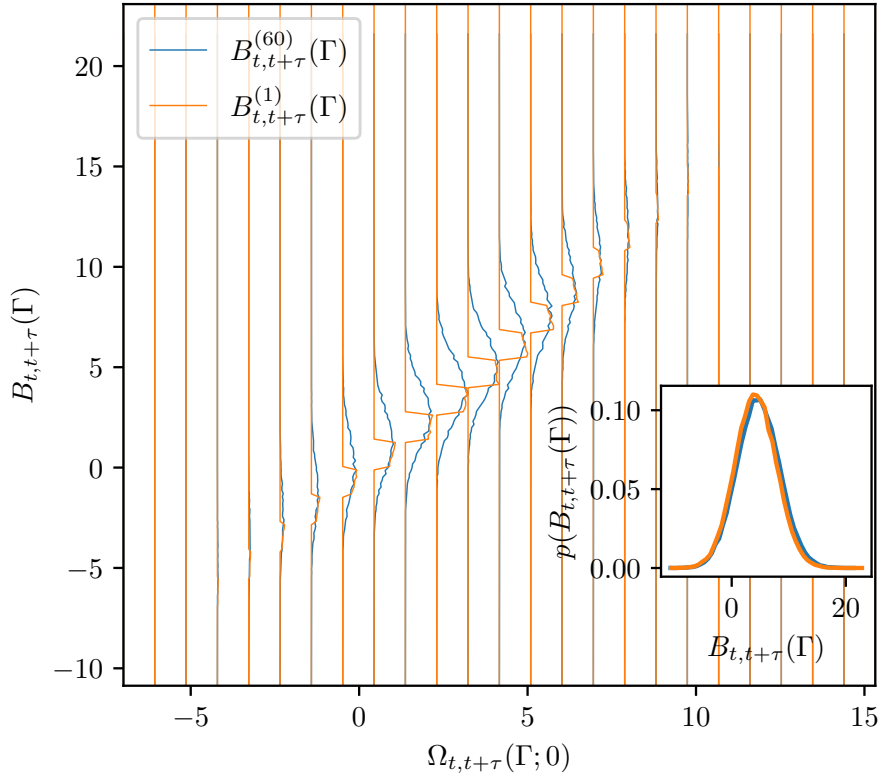


Figure 5. Distribution of $B_{t,t+\tau}^{(N)}(\Gamma)$ given a particular value range of $\Omega_{t,t+\tau}(\Gamma; 0)$ for the optical tweezers simulation with $\rho = 0.4$, $\tau = 6.0$ (see Figure 2 for a comparison of predictive accuracies). Histograms in the main plot are normalised by the peak value for that data set, and are plotted as an offset to the x value. The inset shows the overall distribution of $B_{t,t+\tau}(\Gamma)$ in each case (*i.e.* the sum over all $\Omega_{t,t+\tau}(\Gamma; 0)$ values). Note that $p(B_{t,t+\tau}^{(60)}(\Gamma) < 0)$ is slightly lower than $p(B_{t,t+\tau}^{(1)}(\Gamma) < 0)$, resulting in the slightly higher predictive accuracy of the former. Note also that reversing both axes gives the distribution for reverse trajectories, as does reversing the x axis of the inset.

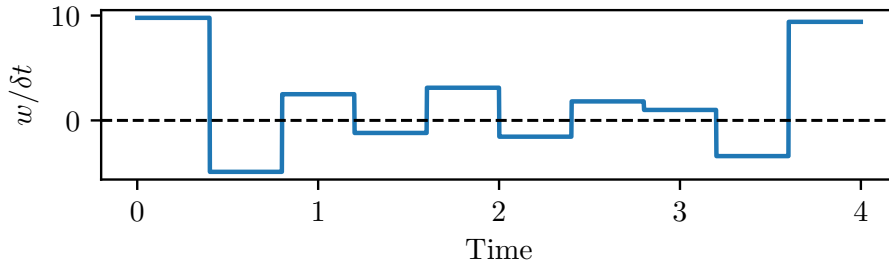


Figure 6. Network weights as a function of the time segment they apply to for a model trained on the optical tweezers dynamics with $\rho = 0.4$ and $\tau = 4.0$ (predictive accuracy shown in Figure 2).

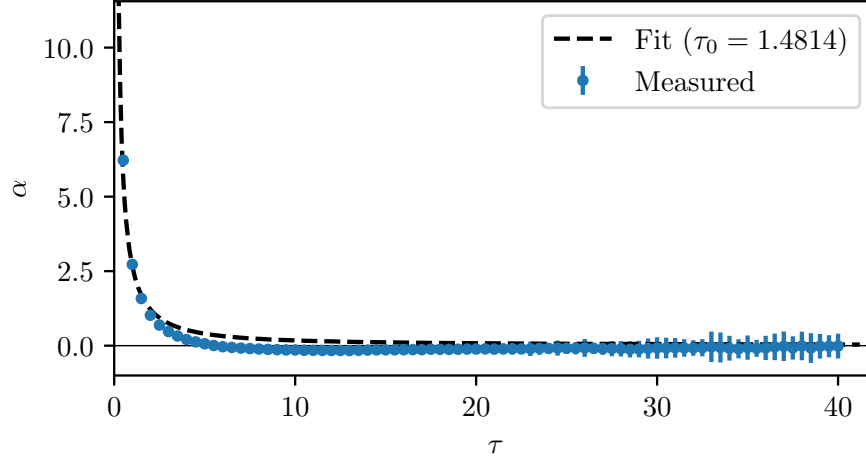


Figure 7. Value of α required for the FT for $(1 + \alpha)\Omega_{t,t+\tau}(\Gamma;0)$ to be best satisfied under the optical tweezers dynamics with $\rho = 0.4$. α was fit to the slope of the FT considering only the inner 50% of A values where statistics are relatively good, but the error bars represent the standard deviation across all available data points. The dashed line represents a fit in the form of Equation 35.

$\Omega_{t,t+\tau}(\Gamma;0)$, and $\Omega_{t+\tau,2t+\tau}(\Gamma;0)$ are linear to a good approximation when $t \rightarrow \infty$.

5.2 Time correlations

If only a single weight (equal to $1 + \alpha$) is required to satisfy an FT, it becomes simple with sufficient data to calculate this weight from the slope of a plot of $\ln[p(\Omega_{t,t+\tau}(\Gamma;0) = A\tau)/p(\Omega_{t,t+\tau}(\Gamma;0) = -A\tau)]$ against $A\tau$. As shown in Figure 7, the required weight as a function of τ is described reasonably well by the equation

$$\alpha(\tau) = \frac{\tau_0 \left(1 - e^{-\tau/\tau_0}\right)}{\tau - \tau_0 \left(1 - e^{-\tau/\tau_0}\right)}, \quad (35)$$

where τ_0 is the time constant of the decay in correlations, as proposed for the space-local FT [22, 23] based on the assumption of exponential decay in spatial correlations (see Equation 15). However, it is notable that for the dynamics modelled, the weights deviate from this form for a range of mid-length trajectories. This deviation (around $\tau = 10$) includes values of $\alpha < 0$, which cannot result from Equation 35. It also corresponds closely to a minima in the autocorrelation function of the instantaneous dissipation function, which similarly represents a region in which the decay in time correlations does not follow an exponential relationship (see Figure S3 in the supporting information). Hence, it appears that derivations based on fitting the autocorrelation function of $\Omega(\Gamma;0)$ could result in a good approximation of α for steady state trajectories, $\Gamma_{t \rightarrow t+\tau}$, provided the fit closely matches the autocorrelation data at a lag of τ (and regardless of whether it is a good fit for other τ values). That is, if only a specific range of τ values is of interest, then a fit to the autocorrelation function of $\Omega(\Gamma;0)$ need only be accurate within that τ range in order to predict values of $\alpha(\tau)$ which satisfy the FT.

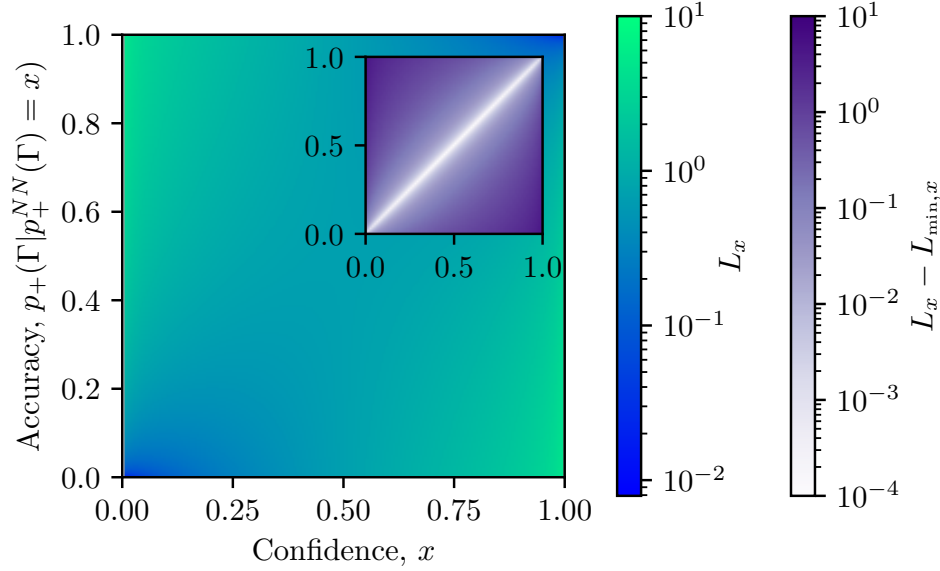


Figure 8. Heat map of $L_x = \langle L(\Gamma) \rangle_{p_+^{NN}(\Gamma)=x}$, the average value of the binary cross-entropy loss function, $L(\Gamma)$, for a given calibration specified by the confidence, x , and accuracy, $p_+(\Gamma|p_+^{NN}(\Gamma) = x)$. A well-calibrated predictor has a confidence equal to its accuracy. The inset shows the difference between L_x and its minimum value for a particular confidence, $L_{\min,x}$, clearly showing that reaching the global minimum of the binary cross-entropy loss function would result in a well-calibrated predictor.

5.3 Calibration

The models in this work were trained to minimise the binary cross-entropy loss for a set of N_t trajectories [17, 34],

$$L = -\frac{1}{N_t} \sum_{i=1}^{N_t} y_i \ln[p_+^{NN}(\Gamma_i)] + (1 - y_i) \ln[1 - p_+^{NN}(\Gamma_i)], \quad (36)$$

where y_i is 1 if the trajectory given by Γ_i is a forward trajectory, or 0 if it has been time-reversed. Hence, for the set of trajectories assigned the particular probability $p_+^{NN}(\Gamma) = x$ of being forward ones by the predictor, the average value of the loss function is given by

$$\langle L \rangle_{p_+^{NN}(\Gamma)=x} = -p_+(\Gamma|p_+^{NN}(\Gamma) = x) \ln(x) - [1 - p_+(\Gamma|p_+^{NN}(\Gamma) = x)] \ln(1 - x), \quad (37)$$

where $p_+(\Gamma|p_+^{NN}(\Gamma) = x)$ is the probability that a trajectory chosen at random from the set was generated by the forward process as opposed to the reverse process (i.e. the accuracy of the predictor for a given confidence). Figure 8 plots $\langle L(\Gamma) \rangle_{p_+^{NN}(\Gamma)=x}$ as a heat map against $p_+(\Gamma|p_+^{NN}(\Gamma) = x)$ and x , clearly showing that the loss function is minimised when $p_+(\Gamma|p_+^{NN}(\Gamma) = x) = x$; that is, when the accuracy matches the confidence. Hence, any model that reaches the global minimum of the binary cross-entropy loss function must be a well-calibrated predictor of time's arrow.

5.4 Proof that a well-calibrated predictor satisfies a fluctuation theorem

Since, from Equations 18 and 23,

$$\begin{aligned} p_+^{NN}(\Gamma) &= \frac{1}{1 + e^{-B_{t,t+\tau}^{(N)}(\Gamma)}}, \\ &= \sigma\left(B_{t,t+\tau}^{(N)}(\Gamma)\right), \end{aligned} \quad (38)$$

the probability that a trajectory with $B_{t,t+\tau}^{(N)}(\Gamma) = A\tau$ is a forward one as opposed to a time-reversed one can be written based on the well-calibrated condition as

$$\begin{aligned} p_+(\Gamma|B_{t,t+\tau}^{(N)}(\Gamma) = A\tau) &= p_+(\Gamma|p_+^{NN}(\Gamma) = \sigma(A\tau)), \\ &= \sigma(A\tau), \\ &= \frac{1}{1 + e^{-A\tau}}. \end{aligned} \quad (39)$$

This can be rearranged to give the ratio

$$\ln \frac{p_+(\Gamma|B_{t,t+\tau}^{(N)}(\Gamma) = A\tau)}{p_-(\Gamma|B_{t,t+\tau}^{(N)}(\Gamma) = A\tau)} = A\tau, \quad (40)$$

noting that $p_+ + p_- = 1$. Since the predictor is well-calibrated, $B_{t,t+\tau}^{(N)}(\Gamma)$ must be odd under time-reversal mapping, and therefore $p_-(\Gamma|B_{t,t+\tau}^{(N)}(\Gamma) = A\tau) = p_+(\Gamma|B_{t,t+\tau}^{(N)}(\Gamma) = -A\tau)$. Furthermore, odd time-reversal symmetry implies that

$$p_+(\Gamma|B_{t,t+\tau}^{(N)}(\Gamma) = A\tau) = \frac{p(B_{t,t+\tau}^{(N)}(\Gamma) = A\tau)}{p(B_{t,t+\tau}^{(N)}(\Gamma) = A\tau) + p(B_{t,t+\tau}^{(N)}(\Gamma) = -A\tau)}, \quad (41)$$

and hence the form of the FT can be recovered:

$$\ln \frac{p(B_{t,t+\tau}^{(N)}(\Gamma) = A\tau)}{p(B_{t,t+\tau}^{(N)}(\Gamma) = -A\tau)} = A\tau. \quad (42)$$

Thus, if Equation 39 holds, the FT (Equation 42) will also be true.

It is therefore evident that any well-calibrated predictor of the direction of time's arrow, will give a function which exactly satisfies the FT. Note that the probability assigned by the predictor need not be calculated directly with the sigmoid function, but could instead be any combination of non-linear functions that is able to produce a well-calibrated prediction. In that case, the inverse sigmoid function of the resultant probability could be used to obtain

$$B_{t,t+\tau}^{(N)}(\Gamma) = -\ln\left(\frac{1}{p_+^{NN}(\Gamma)} - 1\right). \quad (43)$$

For ergodically consistent systems undergoing time-reversible dynamics, there is a non-zero probability that a given trajectory could be a forward or time-reversed one [3], meaning that this function will always be finite if $p_+^{NN}(\Gamma)$ exactly satisfies the well-calibrated condition. However, in practice, small deviations from that condition, or numerical inaccuracy caused by finite precision, may result in some infinite values of $B_{t,t+\tau}^{(N)}(\Gamma)$, and hence the direct inclusion of the sigmoid function in the model is preferable despite not being required.

5.5 Uniqueness

Note in the above derivation that there is no requirement that the predictor is the best possible one for the system. Based on the observations that multiple networks trained on the same system produced different predictors, it appears that there are multiple possible predictors which all satisfy an FT. Indeed, the FT appears to be approximately satisfied for any $B_{t,t+\tau}^{(N)}(\Gamma)$ where the weights are a good representation of the required distribution. It also appears to be satisfied when the weights are re-sampled from that distribution for every trajectory, and when trajectories are randomly permuted (i.e. the same trajectory could produce different values of $B_{t,t+\tau}^{(N^*)}(\Gamma)$ depending on the particular permutation). Since the satisfaction of the FT depends only on the well-calibrated condition, $p_+(\Gamma|p_+^{NN}(\Gamma) = x) = x$, different partitioning of trajectories achieved by different sets of weights (as observed in Figure 5) can all satisfy the FT. Hence, predictors that satisfy the FT appear to be non-unique.

With some thought, this can be seen to apply even to transient systems beginning from a known distribution. Although the definition of the dissipation function is unique and given by Equation 2, the predictors will depend on t_2 .

5.6 Implications of limited information and predictor complexity

Consider the cases where only a linear scaling factor is required for $\Omega_{t,t+\tau}(\Gamma; 0)$ to satisfy an FT to a good approximation; that is,

$$\begin{aligned} B_{t,t+\tau}^{(1)}(\Gamma) &= \left\langle B_{t,t+\tau}^{(N^*)}(\Gamma) \right\rangle = (1 + \alpha)\Omega_{t,t+\tau}(\Gamma; 0), \\ &= \Omega_{t,t+\tau}(\Gamma; 0) + \alpha\Omega_{t,t+\tau}(\Gamma; 0). \end{aligned} \quad (44)$$

The fact that the FT is satisfied to a good approximation might seem at odds with the approximate SSFT,

$$\ln \frac{p(\Omega_{t,t+\tau}(\Gamma; 0) = A\tau)}{p(\Omega_{t,t+\tau}(\Gamma; 0) = -A\tau)} = A\tau + \mathcal{O}(\tau_M). \quad (45)$$

However, this apparent conflict can be reconciled by considering the case in the approximate SSFT where $\Omega_{t,t+\tau}(\Gamma; 0) = 0$. In this case,

$$\begin{aligned} \ln \frac{p(\Omega_{t,t+\tau}(\Gamma; 0) = +0)}{p(\Omega_{t,t+\tau}(\Gamma; 0) = -0)} &= 0 + \mathcal{O}(\tau_M), \\ &= 0, \end{aligned} \quad (46)$$

and hence the error term must have some dependence on $\Omega_{t,t+\tau}(\Gamma; 0)$. As the value calculated by the model in the above cases differs from the dissipation function only by a linear scaling factor, the corresponding FT is

$$\ln \frac{p(\Omega_{t,t+\tau}(\Gamma; 0) = A\tau)}{p(\Omega_{t,t+\tau}(\Gamma; 0) = -A\tau)} = (1 + \alpha)A\tau, \quad (47)$$

which is exactly the form of the space-local FT when a linear correlation between the local and non-local components of the dissipation function is assumed [22, 23]. Hence, the FT satisfied by the model in the single weight case is expected to be an approximate relation, although the approximation appears to be a good one for all systems tested. This, therefore, does not rule out the existence of higher order correlations.

It is notable that a simple scaling factor did not have as high a predictive accuracy as that of a model in which consecutive segments of the dissipation function were used as input (with time ordering preserved).

The root cause of this is difficult to state with certainty, but an analysis of the weights showed that those towards the beginning and end of the trajectory segment were consistently higher than those in the middle. Furthermore, the shape of the weight plot (in the case of longer trajectories, see Figure 6) was found to be qualitatively similar to that of a network with the same structure (but excluding the sigmoid function) when trained to predict the value of the time-local dissipation function for a longer trajectory segment, $\Omega_{t-\Delta\tau, t+\tau+\Delta\tau}(\Gamma; 0)$, given, as in Figure 1a, consecutive segments of $\Omega_{t, t+\tau}(\Gamma; 0)$. This could indicate that the model is taking advantage of learned time correlations to predict slightly longer trajectory segments, and thereby gain more information to enable higher predictive accuracy [31]. It could also be equivalently interpreted as the introduction of non-linear correlations between the local and non-local components of the dissipation function.

Regardless, it is clear that satisfaction of an FT (to a good approximation) does not require full information about the trajectory, and the amount of information available is more strongly correlated with the predictive accuracy than with the accuracy of the FT. Although perhaps surprising at first, a simple thought experiment shows that this is an expected result. Consider a transient system with trajectories of length τ beginning from a known, equilibrium distribution. Given reasonably closely spaced phase points (positions and momenta) along each input trajectory, a sufficiently complex model could learn to effectively integrate the equations of motion to some later time $\tau + \Delta\tau$ and calculate the dissipation function $\Omega_{0, \tau+\Delta\tau}(\Gamma; 0)$. Both $\Omega_{0, \tau}(\Gamma; 0)$ and $\Omega_{0, \tau+\Delta\tau}(\Gamma; 0)$ satisfy the FT, but the latter would give better predictive accuracy due to the extra information available. In practice, though, if used to predict time's arrow for a set of fixed length transient trajectories, such a strategy would not be beneficial. This is because the non-equilibrium driving (and therefore the equations of motion) have some time dependence which must be time-reversed for the reverse trajectories (e.g. turning on the driving at the start of a forward trajectory versus turning it off at the end of a reversed one). The model would first have to determine which direction to integrate the equations of motion before extending the trajectory, thereby requiring the prediction to already be made. However, in a steady state where the non-equilibrium driving process is constant and $t \rightarrow \infty$, both forward and time-reversed trajectories can simply be extended in both directions without issue.

Even with only knowledge of the instantaneous dissipation, and not the precise trajectory, a sufficiently complex model could entirely learn the autocorrelation function of $\Omega(\Gamma; 0)$, and thereby reach a maximal predictive accuracy by capturing all correlations between $\Omega_{t, t+\tau}(\Gamma; 0)$ and $(\Omega_{0, t}(\Gamma; 0) + \Omega_{t+\tau, 2t+\tau}(\Gamma; 0))$. In such a case, it is clear that, similar to Equation 13, the dissipation function from time 0 to time $2t + \tau$, which satisfies the Evans-Searles FT, can be expressed as

$$\Omega_{0, 2t+\tau}(\Gamma; 0) = B(\Omega_{t, t+\tau}(\Gamma; 0)) + \xi(\Gamma), \quad (48)$$

where $B(\Omega_{t, t+\tau}(\Gamma; 0))$ represents the value computed by the model containing all correlations, and $\xi(\Gamma)$ is the remaining uncorrelated component which will depend on the particular trajectory. As $\Omega_{t, t+\tau}(\Gamma; 0)$ is uncorrelated with $\xi(\Gamma)$, $B(\Omega_{t, t+\tau}(\Gamma; 0))$ must also be uncorrelated, and therefore, since $\Omega_{0, 2t+\tau}(\Gamma; 0)$ is odd under time reversal mapping, so must be both B and ξ . Hence, it follows from the functional

FT [1, 20–23] (Equation 10) that

$$\begin{aligned}
\ln \frac{p(\Omega_{t,t+\tau}(\Gamma;0) = A\tau)}{p(\Omega_{t,t+\tau}(\Gamma;0) = -A\tau)} &= -\ln \left\langle e^{-\Omega_{0,2t+\tau}(\Gamma;0)} \right\rangle_{\Omega_{t,t+\tau}(\Gamma;0)=A\tau}, \\
&= -\ln \left\langle e^{-B(\Omega_{t,t+\tau}(\Gamma;0))} e^{-\xi(\Gamma)} \right\rangle_{\Omega_{t,t+\tau}(\Gamma;0)=A\tau}, \\
&= -\ln \left\langle e^{-B(A\tau)} e^{-\xi(\Gamma)} \right\rangle_{\Omega_{t,t+\tau}(\Gamma;0)=A\tau}, \\
&= B(A\tau) - \ln \left\langle e^{-\xi(\Gamma)} \right\rangle, \\
&= B(A\tau),
\end{aligned} \tag{49}$$

where the final line is obtained by noting that since B is an odd function, the term involving the ensemble average must be zero in the $A = 0$ case, and must therefore always be zero as it is uncorrelated with A . This local FT is an exact equality which depends only on time-local information and information that can be obtained with knowledge of the autocorrelation function of $\Omega(\Gamma;0)$, and does not depend on any uncorrelated dissipation. Note that although it is expressed here in terms of time-locality, Equation 49 applies to any local dissipation function that is a component of a global dissipation function which satisfies a FT, including the steady state space-local dissipation function, $\Omega'_{t,t+\tau}(\Gamma;0)$, which is often the easiest to measure experimentally.

5.7 Applications

Finally, it is apparent that optimising the binary cross-entropy loss of a predictor of time's arrow presents a method with which a scaling factor, α , could be calculated for a system of interest and thereby result in a quantity which satisfies a FT to a good approximation. As α depends on both the dynamics and the length of the trajectory segments, calculating it via the slope of a plot of $\ln[p(\Omega_{t,t+\tau}(\Gamma;0) = A\tau)/p(\Omega_{t,t+\tau}(\Gamma;0) = -A\tau)]$ versus $A\tau$ may be infeasible in many cases due to the large number of trajectories required, and similar problems may be encountered in attempting to use the autocorrelation function of $\Omega(\Gamma;0)$ as in Section 5.2 or Equation 49 if correlations decay too slowly. However, testing showed that the logistic regression model converged to a predictor which closely satisfied an FT from very few input trajectories in some cases. For example, training on data from the SLLOD dynamics with $\dot{\gamma} = 0.5$ and $\tau = 0.01$, only 64 input trajectories (32 forward, 32 reverse) were required to calculate a converged value of α . As would be reasonably expected, this required significantly more training epochs than when training on larger data sets (the model needed to 'see' each trajectory more times). However, a converged α value was achieved both in the case of a single-weight model ($N = 1$), and one with $N = 10$ where the samples of the dissipation function were randomly permuted. In the latter case, α was determined by the average of the weights.

One potential problem when calculating α in this manner is that verification by plotting the FT relation requires just as much data as determining it by the slope of a plot of $\ln[p(\Omega_{t,t+\tau}(\Gamma;0) = A\tau)/p(\Omega_{t,t+\tau}(\Gamma;0) = -A\tau)]$ versus $A\tau$. However, this could be avoided by simply increasing the number of input trajectories until the calculated α converges. Note that exact convergence can be difficult to achieve even with a large data set, as there is room for some variance without major impact on the overall predictive accuracy (see Figure 8). However, retraining multiple times on different subsets of the data and averaging over the calculated α values was found to give a good approximation, and a modified loss function that strongly rewards the well-calibrated condition may also prove beneficial. Such a procedure may have applications in predicting the probability of rare events, or in calculating phase variable averages at steady states, although we leave this for future work.

6 Conclusion

Machine learning models were trained to predict whether a given deterministic, nonequilibrium steady state trajectory was one that progressed forward or backward in time. It was found that a value which satisfies a fluctuation theorem can be calculated from the model's output provided the model converged to a well-calibrated predictor (a condition shown to be automatically satisfied if the binary cross-entropy loss is exactly minimised). The FT was satisfied even for very short trajectories where the approximate time-local steady state FT derived from theory is not valid, and this result was verified for a set of common nonequilibrium dynamics at various distances from equilibrium.

It was shown that even a simple linear scaling factor was sufficient to give a good approximation of the FT when applied to the time-local dissipation function defined with respect to the initial (known) phase space distribution. This is equivalent to previously derived space-local FTs. It was also observed that a more complex model was able to capture higher order correlations between the time-local and non-local components of the dissipation function, and thereby produce a higher predictive accuracy. Hence, it was demonstrated that although the amount of information available about the trajectory has some correlation with the predictive accuracy, it had no noticeable effect on the accuracy with which the FT was satisfied for the systems tested. Furthermore, it was demonstrated that an exact local FT can be written which depends only on local information and the correlation between that information and the unknown non-local component. Finally, a method was proposed for calculating the scaling factor required to approximately satisfy the FT in the case that only a small data set is available.

Acknowledgements

The authors thank the Australian Research Council for its support for this project through the Discovery program (FL190100080). We acknowledge access to computational resources provided by the Pawsey Supercomputing Centre with funding from the Australian Government and the government of Western Australia, and the National Computational Infrastructure (NCI Australia), an NCRIS enabled capability supported by the Australian Government. We also acknowledge support from the Queensland Cyber Infrastructure Foundation (QCIF). Finally, we would like to thank Dr. Shern Tee for his insightful comments and suggestions.

References

1. Evans, D. J., Searles, D. J. & Williams, S. R. *Fundamentals of Classical Statistical Thermodynamics* (Wiley-VCH, 2016).
2. Evans, D. J. & Searles, D. J. Equilibrium microstates which generate second law violating steady states. *Phys. Rev. E* **50**, 1645–1648, DOI: [10.1103/PhysRevE.50.1645](https://doi.org/10.1103/PhysRevE.50.1645) (1994).
3. Evans, D. J. & Searles, D. J. The fluctuation theorem. *Adv. Phys.* **51**, 1529–1585, DOI: [10.1080/00018730210155133](https://doi.org/10.1080/00018730210155133) (2002).
4. Evans, D. J. & Morriss, G. P. *Statistical Mechanics of Nonequilibrium Liquids* (Cambridge University Press, 2008), 2nd edn.
5. Evans, D. J., Searles, D. J. & Williams, S. R. On the fluctuation theorem for the dissipation function and its connection with response theory. *J. Chem. Phys.* **128**, 014504, DOI: [10.1063/1.2812241](https://doi.org/10.1063/1.2812241) (2008).

6. Bernardi, S., Brookes, S. J., Searles, D. J. & Evans, D. J. Response theory for confined systems. *J. Chem. Phys.* **137**, 074114, DOI: [10.1063/1.4746121](https://doi.org/10.1063/1.4746121) (2012).
7. Maffioli, L. *et al.* Slip and stress from low shear rate nonequilibrium molecular dynamics: The transient-time correlation function technique. *J. Chem. Phys.* **156**, 184111, DOI: [10.1063/5.0088127](https://doi.org/10.1063/5.0088127) (2022).
8. Yesilata, B., Clasen, C. & McKinley, G. Nonlinear shear and extensional flow dynamics of wormlike surfactant solutions. *J. Non-Newtonian Fluid Mech.* **133**, 73–90, DOI: [10.1016/j.jnnfm.2005.10.009](https://doi.org/10.1016/j.jnnfm.2005.10.009) (2006).
9. Paul, G., Chopkar, M., Manna, I. & Das, P. Techniques for measuring the thermal conductivity of nanofluids: A review. *Renew. Sustain. Energy Rev.* **14**, 1913–1924, DOI: [10.1016/j.rser.2010.03.017](https://doi.org/10.1016/j.rser.2010.03.017) (2010).
10. Palacios, A., Cong, L., Navarro, M., Ding, Y. & Barreneche, C. Thermal conductivity measurement techniques for characterizing thermal energy storage materials – a review. *Renew. Sustain. Energy Rev.* **108**, 32–52, DOI: [10.1016/j.rser.2019.03.020](https://doi.org/10.1016/j.rser.2019.03.020) (2019).
11. Bardeen, C. J. The structure and dynamics of molecular excitons. *Annu. Rev. Phys. Chem.* **65**, 127–148, DOI: [10.1146/annurev-physchem-040513-103654](https://doi.org/10.1146/annurev-physchem-040513-103654) (2014).
12. Balsara, N. P. & Newman, J. Relationship between steady-state current in symmetric cells and transference number of electrolytes comprising univalent and multivalent ions. *J. Electrochem. Soc.* **162**, A2720–A2722, DOI: [10.1149/2.0651514jes](https://doi.org/10.1149/2.0651514jes) (2015).
13. Vogel, C. & Marcotte, E. M. Insights into the regulation of protein abundance from proteomic and transcriptomic analyses. *Nat. Rev. Genet.* **13**, 227–232, DOI: [10.1038/nrg3185](https://doi.org/10.1038/nrg3185) (2012).
14. Montgomery, M. T. & Smith, R. K. Recent developments in the fluid dynamics of tropical cyclones. *Annu. Rev. Fluid Mech.* **49**, 541–574, DOI: [10.1146/annurev-fluid-010816-060022](https://doi.org/10.1146/annurev-fluid-010816-060022) (2017).
15. Carleo, G. *et al.* Machine learning and the physical sciences. *Rev. Mod. Phys.* **91**, 045002, DOI: [10.1103/revmodphys.91.045002](https://doi.org/10.1103/revmodphys.91.045002) (2019).
16. Krenn, M. *et al.* On scientific understanding with artificial intelligence. *Nat. Rev. Phys.* **4**, 761–769, DOI: [10.1038/s42254-022-00518-3](https://doi.org/10.1038/s42254-022-00518-3) (2022).
17. Seif, A., Hafezi, M. & Jarzynski, C. Machine learning the thermodynamic arrow of time. *Nat. Phys.* **17**, 105–113, DOI: [10.1038/s41567-020-1018-2](https://doi.org/10.1038/s41567-020-1018-2) (2021).
18. Evans, D. J. & Searles, D. J. Causality, response theory, and the second law of thermodynamics. *Phys. Rev. E* **53**, 5808–5815, DOI: [10.1103/PhysRevE.53.5808](https://doi.org/10.1103/PhysRevE.53.5808) (1996).
19. Coretti, A., Rondoni, L. & Bonella, S. Fluctuation relations for dissipative systems in constant external magnetic field: Theory and molecular dynamics simulations. *Entropy* **23**, 146, DOI: [10.3390/e23020146](https://doi.org/10.3390/e23020146) (2021).
20. Searles, D. J., Ayton, G. & Evans, D. J. Generalized fluctuation formula. *AIP Conf. Proc.* **519**, 271–280, DOI: [10.1063/1.1291568](https://doi.org/10.1063/1.1291568) (2000).
21. Searles, D. J., Johnston, B. M., Evans, D. J. & Rondoni, L. Time reversibility, correlation decay and the steady state fluctuation relation for dissipation. *Entropy* **15**, 1503–1515, DOI: [10.3390/e15051503](https://doi.org/10.3390/e15051503) (2013).
22. Talaei, Z., Reid, J. C. & Searles, D. J. A local dissipation theorem. *J. Chem. Phys.* **137**, 214110, DOI: [10.1063/1.4768897](https://doi.org/10.1063/1.4768897) (2012).

23. Michel, G. & Searles, D. J. Local fluctuation theorem for large systems. *Phys. Rev. Lett.* **110**, 260602, DOI: [10.1103/PhysRevLett.110.260602](https://doi.org/10.1103/PhysRevLett.110.260602) (2013).
24. Shang, X. D., Tong, P. & Xia, K. Q. Test of steady-state fluctuation theorem in turbulent Rayleigh-Bénard convection. *Phys. Rev. E* **72**, 6–9, DOI: [10.1103/PhysRevE.72.015301](https://doi.org/10.1103/PhysRevE.72.015301) (2005).
25. Ayton, G., Evans, D. J. & Searles, D. J. A local fluctuation theorem. *J. Chem. Phys.* **115**, 2033–2037, DOI: [10.1063/1.1385158](https://doi.org/10.1063/1.1385158) (2001).
26. Feitosa, K. & Menon, N. Fluidized granular medium as an instance of the fluctuation theorem. *Phys. Rev. Lett.* **92**, 164301, DOI: [10.1103/PhysRevLett.92.164301](https://doi.org/10.1103/PhysRevLett.92.164301) (2004).
27. Gallavotti, G. A local fluctuation theorem. *Physica A* **263**, 39–50, DOI: [10.1016/S0378-4371\(98\)00502-0](https://doi.org/10.1016/S0378-4371(98)00502-0) (1999).
28. Crooks, G. E. Entropy production fluctuation theorem and the nonequilibrium work relation. *Phys. Rev. E* **60**, 2721–2726, DOI: [10.1103/PhysRevE.60.2721](https://doi.org/10.1103/PhysRevE.60.2721) (1999).
29. Jarzynski, C. Equalities and inequalities: Irreversibility and the Second Law of Thermodynamics at the nanoscale. *Annu. Rev. Condens. Matter Phys.* **2**, 329–351, DOI: [10.1146/annurev-conmatphys-062910-140506](https://doi.org/10.1146/annurev-conmatphys-062910-140506) (2011).
30. Paneni, C., Searles, D. J. & Rondoni, L. Temporal asymmetry of fluctuations in nonequilibrium steady states. *J. Chem. Phys.* **124**, 114109, DOI: [10.1063/1.2171964](https://doi.org/10.1063/1.2171964) (2006).
31. Paneni, C., Searles, D. J. & Rondoni, L. Temporal asymmetry of fluctuations in nonequilibrium steady states: Links with correlation functions and nonlinear response. *J. Chem. Phys.* **128**, 164515, DOI: [10.1063/1.2894471](https://doi.org/10.1063/1.2894471) (2008).
32. Wang, G. M. *et al.* Experimental study of the fluctuation theorem in a nonequilibrium steady state. *Phys. Rev. E* **71**, 046142, DOI: [10.1103/PhysRevE.71.046142](https://doi.org/10.1103/PhysRevE.71.046142) (2005).
33. Kingma, D. P. & Ba, J. L. Adam: A method for stochastic optimization. In *3rd International Conference on Learning Representations, ICLR 2015 - Conference Track Proceedings* (2015).
34. Goodfellow, I., Bengio, Y. & Courville, A. *Deep Learning* (MIT Press, 2016). <http://www.deeplearningbook.org>.
35. Hoover, W. G. Canonical dynamics: Equilibrium phase-space distributions. *Phys. Rev. A* **31**, 1695–1697, DOI: [10.1103/PhysRevA.31.1695](https://doi.org/10.1103/PhysRevA.31.1695) (1985).
36. Wang, G. M., Sevick, E. M., Mittag, E., Searles, D. J. & Evans, D. J. Experimental demonstration of violations of the Second Law of Thermodynamics for small systems and short time scales. *Phys. Rev. Lett.* **89**, 050601, DOI: [10.1103/PhysRevLett.89.050601](https://doi.org/10.1103/PhysRevLett.89.050601) (2002).
37. Weeks, J. D., Chandler, D. & Andersen, H. C. Role of repulsive forces in determining the equilibrium structure of simple liquids. *J. Chem. Phys.* **54**, 5237–5247, DOI: [10.1063/1.1674820](https://doi.org/10.1063/1.1674820) (1971).
38. Sarman, S. S., Evans, D. J. & Cummings, P. T. Recent developments in non-Newtonian molecular dynamics. *Phys. Rep.* **305**, 1–92, DOI: [10.1016/S0370-1573\(98\)00018-0](https://doi.org/10.1016/S0370-1573(98)00018-0) (1998).
39. Lees, A. W. & Edwards, S. F. The computer study of transport processes under extreme conditions. *J. Phys. C: Solid State Phys.* **5**, 1921–1929, DOI: [10.1088/0022-3719/5/15/006](https://doi.org/10.1088/0022-3719/5/15/006) (1972).
40. Evans, D. J., Searles, D. J. & Williams, S. R. The covariant dissipation function for transient nonequilibrium states. *J. Chem. Phys.* **133**, 054507, DOI: [10.1063/1.3463439](https://doi.org/10.1063/1.3463439) (2010).

41. Petersen, C. F., Evans, D. J. & Williams, S. R. The instantaneous fluctuation theorem. *J. Chem. Phys.* **139**, 184106, DOI: [10.1063/1.4829445](https://doi.org/10.1063/1.4829445) (2013).

Supporting Information: Machine learning a time-local fluctuation theorem for nonequilibrium steady states

Stephen Sanderson¹, Charlotte F. Petersen^{1,2}, and Debra J. Searles^{1,3,*}

¹Australian Institute for Bioengineering and Nanotechnology, The University of Queensland, Brisbane, QLD, 4072, Australia

²School of Chemistry, University of Melbourne, Melbourne, Victoria, 3010, Australia

³School of Chemistry and Molecular Biosciences, The University of Queensland, Brisbane, QLD, 4072, Australia

*d.bernhardt@uq.edu.au

1 Derivation of $p_+(\Gamma_{0 \rightarrow \tau})$ from the fluctuation theorem

Consider configurations sampled from an initial equilibrium state that evolve with a given protocol to configurations that would sample a new equilibrium state, if allowed to relax. Let the free energy difference in these equilibrium states be ΔF . The Crooks fluctuation theorem states that

$$\frac{p_F(W_F = A)}{p_R(W_R = -A)} = e^{\beta(A - \Delta F)}, \quad (\text{S1})$$

where $p_F(W_F = A)$ is the probability of observing the value, A , of the work when driving a system from the initial equilibrium ensemble to the final configuration and the probability, $p_R(W_R = -A)$, is then the probability of observing the value of work, $-A$, when driving the system from the equilibrium distribution of the final configuration back to the initial configuration, under the reverse protocol. This relationship can be obtained by considering the ratio of probabilities of observing forward trajectories within a phase volume, $\delta\Gamma$, about point Γ_0 , sampled from the initial equilibrium ensemble; compared to the probability of observing ‘reverse’ trajectories in the phase volume it would evolve to, Γ_τ , subject to a time reversal mapping ($\Gamma_0^* = M^T(\Gamma_\tau)$) and evolved using the reverse protocol. This gives, [1, 2]

$$\frac{p_F(\delta\Gamma_0)}{p_R(\delta\Gamma_0^*)} = \frac{p_F(\Gamma_{0 \rightarrow \tau})}{p_R(\Gamma_{0 \rightarrow \tau}^*)} = e^{\beta(W(\Gamma_{0 \rightarrow \tau}) - \Delta F)}. \quad (\text{S2})$$

Consider a mix of trajectories in which an equal number were generated by the forward process and reverse process, with the reverse trajectories then played backwards. The probability that a given trajectory was generated by the forward one rather than the reverse one is given by

$$p_+(\Gamma_{0 \rightarrow \tau}) = \frac{p_F(\Gamma_{0 \rightarrow \tau})}{p_F(\Gamma_{0 \rightarrow \tau}) + p_R(\Gamma_{\tau \rightarrow 0})}, \quad (\text{S3})$$

where $p_R(\Gamma_{\tau \rightarrow 0}) = p_R(\Gamma_{0 \rightarrow \tau}^*)$ is the probability that the trajectory was generated by the reverse process, and is played backwards. Then,

$$p_+(\Gamma_{0 \rightarrow \tau}) = \frac{p_F(\Gamma_{0 \rightarrow \tau})}{p_F(\Gamma_{0 \rightarrow \tau}) + p_R(\Gamma_{0 \rightarrow \tau}^*)}, \quad (\text{S4})$$

$$= \frac{p_F(\Gamma_{0 \rightarrow \tau})}{p_F(\Gamma_{0 \rightarrow \tau}) + p_F(\Gamma_{0 \rightarrow \tau})e^{-\beta(W(\Gamma_{0 \rightarrow \tau}) - \Delta F)}}, \quad (\text{S5})$$

$$= \frac{1}{1 + e^{-\beta(W(\Gamma_{0 \rightarrow \tau}) - \Delta F)}}. \quad (\text{S6})$$

Using the same logic, an equivalent expression can be derived from the Evans-Searles fluctuation theorem. [3] That is, the arguments leading to the Evans-Searles fluctuation theorem give:

$$\frac{p(\delta\Gamma_0)}{p(\delta\Gamma_0^*)} = \frac{p(\Gamma_{0\rightarrow\tau})}{p(\Gamma_{0\rightarrow\tau}^*)} = e^{\Omega_{0,\tau}(\Gamma;0)}. \quad (\text{S7})$$

Then, assuming an equal mix of forward and time-reversed trajectories, this expression can then be rearranged as before to give the probability that a trajectory is a forward one as

$$p_+(\Gamma_{0\rightarrow\tau}) = \frac{1}{1 + e^{-\Omega_{0,\tau}(\Gamma;0)}}. \quad (\text{S8})$$

2 Illustration of typical forward and reverse trajectories

Figure S1 represents the relationships between the time-evolution of the dissipation function along trajectories that are played in the forward and reverse directions, and the likelihood of them being observed for a typical driven system, initially at equilibrium and reaching a steady state. The dissipation function would be expected to obey a fluctuation theorem as presented in Equation 1 of the main text.

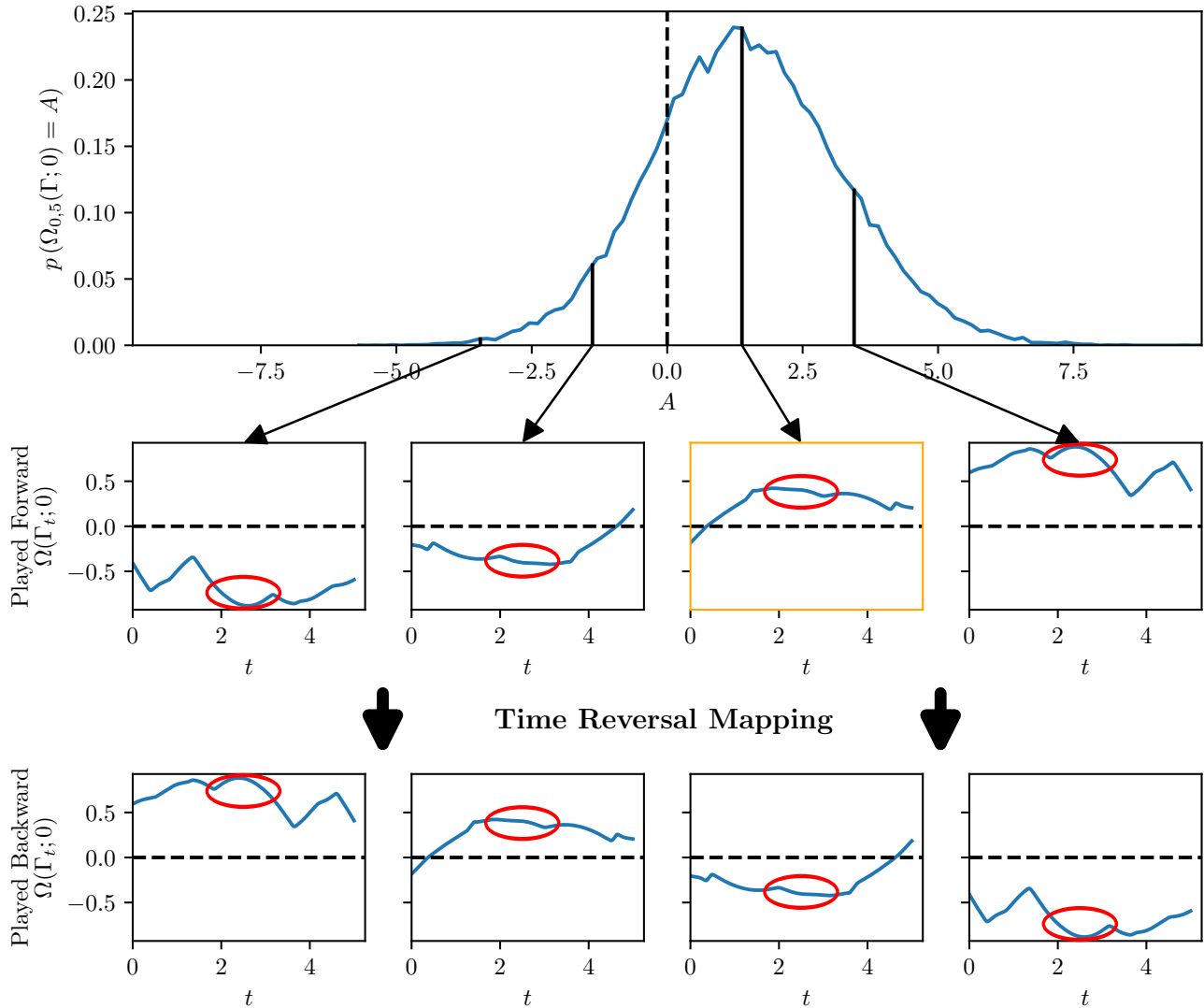


Figure S1. Schematic diagram illustrating the probability distribution of the dissipation of trajectories $\Gamma_{0 \rightarrow 5}$, typical trajectories generated when a driving force is applied at $t = 0$, and the trajectories that would be observed if the original set were played backwards. The four representative plots of the instantaneous dissipation function against time are arranged by the trajectories' value of A , as indicated. The bottom four plots illustrate what these same trajectories would look like if played in reverse. The trace highlighted in orange is a trajectory that would be typical of the forward process. The circled regions represent portions of steady state trajectories. This diagram was generated using transient trajectories from the optical tweezers experiment with a fluid number density of $\rho = 0.3$, $k_{\text{trap}} = 1.0$, $v_{\text{trap}} = 0.5$, and $k_B T = 1.0$.

3 Benchmarking for deterministic transient systems

Linear regression models were trained on transient trajectories obtained using non-equilibrium simulations of the optical trap system beginning from an equilibrium state. These transient trajectories all began from different initial conditions taken at regular time intervals from the equilibrium system. While various input data was trialed, the only input that mattered under this simple model was the position of the trapped particle, x , in the direction that the trap was moving, which is directly related to the instantaneous dissipation function for these dynamics. Samples of x were taken at regular time intervals. Figure S2a shows that the network trained best when given enough samples of the trajectory to have near-complete information while keeping the number of free parameters to a minimum. As this figure was generated using the position of the particle relative to the *initial* position of the trap, a bias was required to achieve good results. The fit of the model's output for the best-performing sampling period was then compared in Figure S2b to the relation expected based on the Evans-Searles fluctuation theorem (Eqn. S8), and found to be in good agreement.

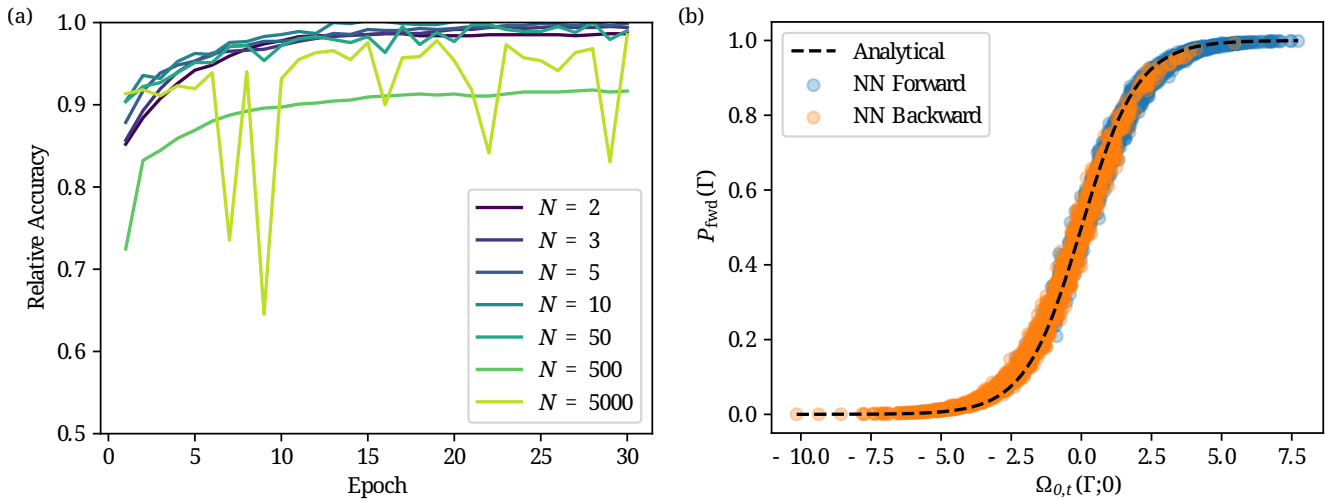


Figure S2. (a) Training accuracy for N instantaneous samples of the trapped particle's position along each transient deterministic trajectory, and (b) model predictions plotted in comparison to Equation S8 for $N = 10$, where blue circles represent trajectories that were played forwards, and orange those that were played backwards. Trajectories were generated with the transient optical tweezers dynamics (beginning from equilibrium) for $\rho = 0.3$, $v_{\text{trap}} = 0.5$, $k_{\text{trap}} = 1.0$, and $k_B T = 1.0$.

4 Autocorrelation of the instantaneous dissipation function

Figure S3 shows the autocorrelation function of the instantaneous dissipation function at steady state for the same dynamics used to plot Figure 5c in the main text. Note the deviation from an exponential decay near $\Delta\tau = 10$ corresponds closely with the region of Figure 5c in which the assumption of an exponential decay in correlations does not produce a good fit for α .

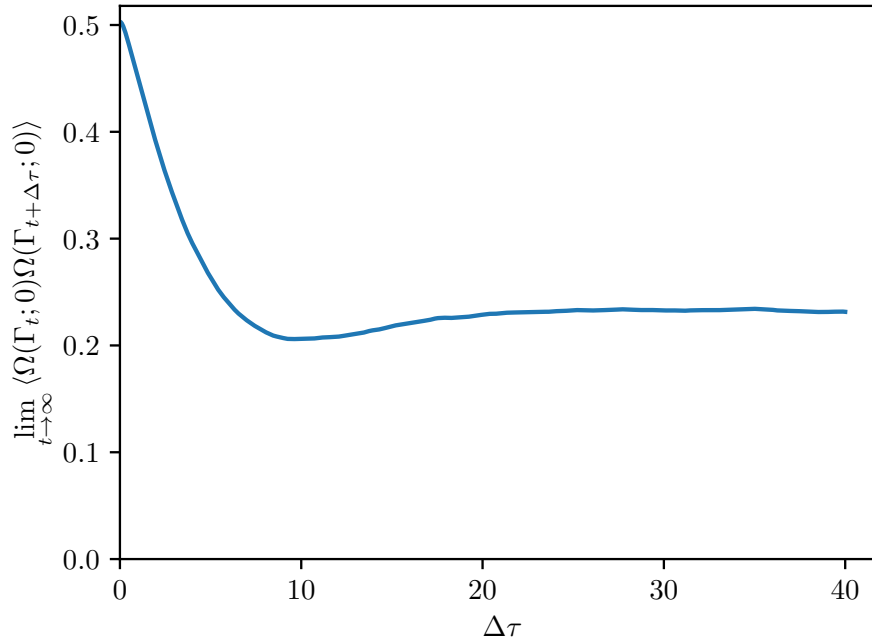


Figure S3. Autocorrelation function of the instantaneous dissipation function, $\Omega(\Gamma_t; 0)$, calculated from 100,000 repetitions of the optical tweezers dynamics with $\rho = 0.4$, $v_{\text{trap}} = 0.5$, $k_{\text{trap}} = 1.0$, and $k_B T = 1.0$.

References

1. Jarzynski, C. Equalities and inequalities: Irreversibility and the Second Law of Thermodynamics at the nanoscale. *Annu. Rev. Condens. Matter Phys.* **2**, 329–351, DOI: [10.1146/annurev-conmatphys-062910-140506](https://doi.org/10.1146/annurev-conmatphys-062910-140506) (2011).
2. Davie, S. J., Reid, J. C. & Searles, D. J. The free energy of expansion and contraction: Treatment of arbitrary systems using the jarzynski equality. *J. Chem. Phys.* **136**, 174111, DOI: [10.1063/1.4707348](https://doi.org/10.1063/1.4707348) (2012).
3. Evans, D. J. & Searles, D. J. The fluctuation theorem. *Adv. Phys.* **51**, 1529–1585, DOI: [10.1080/00018730210155133](https://doi.org/10.1080/00018730210155133) (2002).